NAVAL POSTGRADUATE SCHOOL

MONTEREY, CALIFORNIA

THESIS

MODELING AND SIMULATIONS ON THE EFFECTS OF SHORTWAVE ENERGY ON MICROPARTICLE AND NANOPARTICLE FILLED COMPOSITES

by

Scott R. Delwiche

June 2014

Thesis Advisor: Young W. Kwon
Co-Advisor: Dragoslav Grbovic

Approved for public release; distribution is unlimited

THIS PAGE INTENTIONALLY LEFT BLANK

REPORT DOCUMENTATION PAGE

Form Approved OMB No. 0704–0188

1. AGENCY USE ONLY *(Leave blank)*	2. REPORT DATE	3. REPORT TYPE AND DATES COVERED
	June 2014	Master's Thesis

4. TITLE AND SUBTITLE
MODELING AND SIMULATIONS ON THE EFFECTS OF SHORTWAVE ENERGY ON MICROPARTICLE AND NANOPARTICLE FILLED COMPOSITES

5. FUNDING NUMBERS

6. AUTHOR(S) Scott R. Delwiche

7. PERFORMING ORGANIZATION NAME(S) AND ADDRESS(ES)
Naval Postgraduate School
Monterey, CA 93943–5000

8. PERFORMING ORGANIZATION REPORT NUMBER

9. SPONSORING /MONITORING AGENCY NAME(S) AND ADDRESS(ES)
N/A

10. SPONSORING/MONITORING AGENCY REPORT NUMBER

11. SUPPLEMENTARY NOTES The views expressed in this thesis are those of the author and do not reflect the official policy or position of the Department of Defense or the U.S. Government. IRB Protocol number ____N/A____.

12a. DISTRIBUTION / AVAILABILITY STATEMENT
Approved for public release; distribution is unlimited

12b. DISTRIBUTION CODE
A

13. ABSTRACT (maximum 200 words)

This research focused on the experimentation and modeling of a series of micro- and nanoparticles in a variety of media and the response of those materials to terahertz (THz) electromagnetic waves.

A series of experiments tested the response of aluminum microspheres, nickel microspheres and carbon nanotubes (CNTs) in epoxy, liquid tape or SPR955 positive photoresist to THz radiation from 5 THz to 18 THz. The experimental results showed the absorption characteristics of the micro- and nanoparticles, as well as the media used. The Transfer Matrix Method was used to obtain values for the real and imaginary portions of the refractive index of the photoresist to be used in the finite element modeling of the composites.

A series of finite element models was built using the experimentally derived data and simulated from 5 THz to 18 THz. The models tested various geometries and numbers of particles as well as different thicknesses of the media. The modeling determined that the absorption characteristics seen experimentally were a function of geometry and particle size. Accurate models can be built of aluminum micro particles in photoresist for the frequency spectrum between 10 and 18 THZ.

14. SUBJECT TERMS Carbon nanotubes, Terahertz, THz, Microparticles, Nanoparticles	15. NUMBER OF PAGES
	79
	16. PRICE CODE

17. SECURITY CLASSIFICATION OF REPORT	18. SECURITY CLASSIFICATION OF THIS PAGE	19. SECURITY CLASSIFICATION OF ABSTRACT	20. LIMITATION OF ABSTRACT
Unclassified	Unclassified	Unclassified	UU

NSN 7540–01–280–5500

Standard Form 298 (Rev. 2–89)
Prescribed by ANSI Std. 239–18

THIS PAGE INTENTIONALLY LEFT BLANK

Approved for public release; distribution is unlimited

MODELING AND SIMULATIONS ON THE EFFECTS OF SHORTWAVE ENERGY ON MICROPARTICLE AND NANOPARTICLE FILLED COMPOSITES

Scott R. Delwiche
Lieutenant Commander, United States Navy
B.S, United States Naval Academy, 2002
M.S.E., Catholic University, 2008

Submitted in partial fulfillment of the
requirements for the degree of

MASTER OF SCIENCE IN MECHANICAL ENGINEERING

from the

NAVAL POSTGRADUATE SCHOOL
June 2014

Author: Scott R. Delwiche

Approved by: Young W. Kwon, Ph.D.
Thesis Advisor

Dragoslav Grbovic, Ph.D.
Co-Advisor

Knox T. Millsaps, Ph.D.
Chair, Department of Mechanical and Aerospace Engineering

THIS PAGE INTENTIONALLY LEFT BLANK

ABSTRACT

This research focused on the experimentation and modeling of a series of micro- and nanoparticles in a variety of media and the response of those materials to terahertz (THz) electromagnetic waves.

A series of experiments tested the response of aluminum microspheres, nickel microspheres and carbon nanotubes (CNTs) in epoxy, liquid tape or SPR955 positive photoresist to THz radiation from 5 THz to 18 THz. The experimental results showed the absorption characteristics of the micro- and nanoparticles, as well as the media used. The Transfer Matrix Method was used to obtain values for the real and imaginary portions of the refractive index of the photoresist to be used in the finite element modeling of the composites.

A series of finite element models was built using the experimentally derived data and simulated from 5 THz to 18 THz. The models tested various geometries and numbers of particles as well as different thicknesses of the media. The modeling determined that the absorption characteristics seen experimentally were a function of geometry and particle size. Accurate models can be built of aluminum micro particles in photoresist for the frequency spectrum between 10 and 18 THZ.

THIS PAGE INTENTIONALLY LEFT BLANK

TABLE OF CONTENTS

I. INTRODUCTION....1
A. OVERVIEW....1
1. Carbon Nanotubes, Aluminum Microparticles, and Nickel Microparticles....2
2. Terahertz Technology....3
B. THESIS OBJECTIVES....3

II. EXPERIMENTAL SAMPLE PREPARATION....5
A. SAMPLE PREPARATION: MOLDS USED....5
1. Epoxy-Based Substrate Mold....5
2. Silicon Wafer Mold Used with Photoresist Solution....7
3. Silicon Wafer Sandwich Mold....8
B. SAMPLE PREPARATION: MEDIA....8
1. Epoxy as a Medium....9
2. Liquid Tape as a Medium with a Silicon Wafer as a Substrate....11
3. Photoresist....14
4. Various Nanoparticles in Air....14

III. EXPERIMENTAL RESULTS AND ANALYSIS....17
A. FTIR OPERATION....17
B. RESULTS....21
1. Epoxy as a Medium....21
2. Liquid Tape as a Medium....26
3. Photoresist as a Medium....27
4. Various Particles in Air....30
C. DETERMINATION OF REFRACTIVE INDEX....35

IV. MODELING....39
A. COMSOL RF MODULE....39
B. MODELING A SINGLE UNIT CELL....40
1. Medium and Substrate Models....43
2. A Single Microsphere in a Thin Medium....44
3. Various Numbers of Aluminum Spheres in Photoresist Solution....46

V. CONCLUSIONS....55

APPENDIX. DETERMINATION OF REFRACTIVE INDEX FOR ALUMINUM....57

LIST OF REFERENCES....59

INITIAL DISTRIBUTION LIST....61

THIS PAGE INTENTIONALLY LEFT BLANK

LIST OF FIGURES

Figure 1 Chart of the Complete Electromagnetic Spectrum, from [2] 1
Figure 2 Aluminum Mold Used For Epoxy Based Samples 6
Figure 3 Silicon Wafer Mold, with Two Windows, for Photoresist Solution 7
Figure 4 Silicon Sandwich Mold for Various Nano- and Microparticles 8
Figure 5 Epoxy-Based Samples with Various Percentages of CNTs 10
Figure 6 SEM Images of Nickel Powder with Nominal 5 μm Diameter Spheres at (a) 500x Magnification and (b) 4000x Magnification 10
Figure 7 Epoxy-Based Samples with Nickel 5 μm Diameter Nanoparticles 11
Figure 8 Liquid Tape Applied with a Spin Coater Onto a 300 μm Thick, 10.16 cm (4 in) Diameter Silicon Wafer 12
Figure 9 SEM Images of Aluminum Power with Nominal 20 μm Spheres at (a) 100x and (b) 500x Magnification 12
Figure 10 Liquid Tape Mixed with 20 μm Aluminum Nanoparticles, Applied with a Spin Coater, on a 300 μm Silicon Wafer 13
Figure 11 SEM Images of Sputter Coated Liquid Tape Sample with Nominal 20 μm Diameter Aluminum Spheres in Liquid Tape Showing Clumping, Seen at (a) 100x and (b) 500x 14
Figure 12 500 μm Thick Silicon Wafer Mold with 20 μm Aluminum Powder and 5 μm Nickel Powder 15
Figure 13 Thermo Scientific Nexus 870 FTIR Spectrometer 17
Figure 14 AutoPro5 Interface 18
Figure 15 (a) FTIR set up to measure reflection, from [16] (b) FTIR set up to measure transmission, from [16] 19
Figure 16 Multiple-Beam Interference Pattern (Fabry-Perot Effect) Due to Constructive and Destructive Interference, after [17] 20
Figure 17 Epoxy Only Sample Data Collection Points 21
Figure 18 Experimentally Obtained Reflection, Transmission and Absorption Values of 2mm Thick Epoxy-Only Sample 22
Figure 19 Absorption of THz Radiation in Epoxy with 10% CNTs 23
Figure 20 Absorption Due Only to CNTs 24
Figure 21 Absorption Characteristics of 4% (by Weight), 5 μm Diameter Nickel Spheres in Epoxy 25
Figure 22 Absorption Due Only to 5 μm Nickel Particles 25
Figure 23 Absorption Characteristics of a Thin Layer of Liquid Tape on a 300 μm Silicon Wafer 26
Figure 24 Absorption Characteristics of Liquid Tape with 20% Aluminum Spheres on a 300 μm Silicon Wafer 27
Figure 25 Absorption of Only 20 μm Aluminum Spheres 27
Figure 26 Averaged Absorption of Photoresist Only 29
Figure 27 Averaged Absorption of Photoresist with 20 μm Aluminum Particles 29
Figure 28 Averaged Absorption of 20 μm Aluminum Particles Alone 30

Figure 29 Absorption Characteristics of the Average of Three Sample Points on the Silicon Sandwich Mold, Blank Window 31
Figure 30 Averaged Absorption Characteristics of Multi-Walled CNTs in Air in the Silicon Sandwich Mold....31
Figure 31 Averaged Absorption Due Only to Multiwall CNTs with Size Characteristics as Found in Table 1 32
Figure 32 Absorption of 20 μm Aluminum Spheres in Air, in Silicon Wafer Sandwich Mold 33
Figure 33 Absorption Due only to 20 μm Aluminum Spheres 34
Figure 34 Average Absorption of 5 μm Nickel Spheres in Air, in Silicon Wafer Sandwich Mold 35
Figure 35 Average Absorption Due Only to 5 μm Nickel Spheres....35
Figure 36 (a) Simulated Reflection, Transmission and Absorption in Transfer Matrix Method GUI (b) Experimental Reflection, Transmission, and Absorption in Transfer Matrix Method GUI 37
Figure 37 Thin Film Analysis Values and Linear Fit for SPR955 Real Portion of Refractive Index....37
Figure 38 Thin Film Analysis Values and Second Order Polynomial Best Fit for SPR955 Imaginary Portion of Refractive Index 38
Figure 39 Schematic of 3D Finite Element Model of a Unit Cell Consisting of a Single Aluminum Sphere in Liquid Tape 41
Figure 40 Absorption Characteristics of a Thin Layer of Liquid Tape with Thicknesses Varying from 12 μm to 18 μm 44
Figure 41 Absorption Characteristics of a 16 μm Layer of Liquid Tape 44
Figure 42 COMSOL Models of One 20 μm Aluminum Sphere in 16 μm of Liquid Tape....45
Figure 43 Experimental and COMSOL Results for Absorption in Liquid Tape with 20 μm Diameter Aluminum Spheres 46
Figure 44 Absorption Characteristics of Two, Four, Five, Six and Nine 20 μm Spheres....48
Figure 45 Basic COMSOL Model for Six Aluminum Spheres in Photoresist Solution ..49
Figure 46 Absorption Characteristics of Six Spheres in Photoresist Utilizing Various Refractive Indices 50
Figure 47 COMSOL Results for the Absorption of Six Aluminum Spheres in Photoresist, with Spheres Ranging from 20 μm to 40 μm 51
Figure 48 Composite Graph of Absorption Characteristics of 20, 30 and 40 μm Aluminum Spheres....51
Figure 49 500x SEM Image of Aluminum Powder Showing a Range of Particle Sizes 52
Figure 50 (a) Resistive Heating Losses (in W/m^3) for Six Spheres at 13 THz (b) Resistive Heating Losses (in W/m^3)for Nine Spheres at 13.8 THz 53
Figure 51 Values and Equations Used for the Real Portion of the Refractive Index of Aluminum 57
Figure 52 Values and Equations Used for the Imaginary Portion of the Refractive Index of Aluminum....57

LIST OF TABLES

Table 1 Multiwall CNTs Characteristics Used in Epoxy Samples 9
Table 2 Mass and Types of Particles Used in Silicon Wafer Sandwich Mold 15

THIS PAGE INTENTIONALLY LEFT BLANK

LIST OF ACRONYMS AND ABBREVIATIONS

CNF	carbon nanofiber
CNT	carbon nanotube
CSV	comma separated variables
FTIR	Fourier Transform Infrared Spectroscopy
GUI	Graphical User Interface
NPS	Naval Postgraduate School
SEM	scanning electron microscope
SRL	Sensor Research Laboratory
THz	Terahertz

THIS PAGE INTENTIONALLY LEFT BLANK

ACKNOWLEDGMENTS

I would like to thank Prof. Young Kwon and Prof. Dragoslav Grbovic for their efforts and support over the course of my research. Their knowledge was vital throughout the research. I would also like to thank Dr. Sarath Menon for his help with the SEM and assisting with all of my imaging needs.

And finally, I would like to thank my wife and children for their support while I spent the time required to complete my research.

THIS PAGE INTENTIONALLY LEFT BLANK

I. INTRODUCTION

A. OVERVIEW

Particles in the nano- and micro-scale are of great interest to researchers in academia and in the commercial realm. As technology continues to evolve, it becomes easier to characterize the mechanical properties of the particles and their interaction with other materials. The Navy is one entity that is also focusing a large amount of research effort into incorporating nanoparticles such as carbon nanotubes (CNTs) into many different applications such as sensors, armor, composites, and explosives.

Another realm of technology that is receiving a renewed interest is the part of the electromagnetic spectrum between microwaves and the infrared region, known as the far infrared or the terahertz (THz) range, which is between 100 GHz and 30 THz, and seen in Figure 1. It has been studied in fields such as astronomy and analytical science for many years in the past, but due to recent advancements in nanotechnology and photonics, THz technology is seeing use in many different applications. Some of these applications include information and communications technology, non-destructive evaluation, global environmental monitoring and ultrafast computing [1].

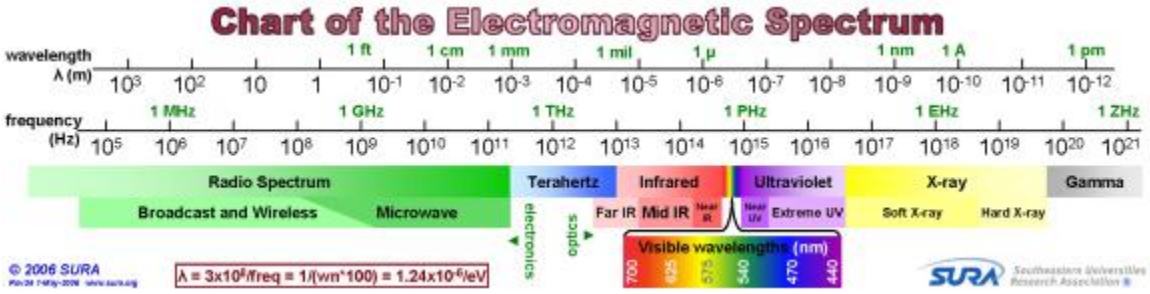

Figure 1 Chart of the Complete Electromagnetic Spectrum, from [2]

Since both of these technologies are being explored and used at an increased rate, it is important to understand if there are any important interactions that occur between them as it is very likely that some form of THz sensing will be used on materials

containing micro- and nanoparticles. These interactions can help identify any vulnerabilities that may present themselves as a result of the interactions.

1. Carbon Nanotubes, Aluminum Microparticles, and Nickel Microparticles

One of the great discoveries in the realm of nanotechnology was the discovery of CNTs. This discovery is largely credited to Sumio Iijima in 1991 in a letter written to the magazine *Nature* [3]. Since then, much research has been conducted in the field of CNTs. Current research at the Naval Postgraduate School (NPS) is focused on using various nanoparticles and nanotubes for applications in energy generation, composites, sensors and armor.

Some specific examples are the use of CNTs for the construction and the repair of ships as part of composite patches [4], [5]. Composites that are epoxy-based are frequently utilized in many applications due to their qualities such as high modulus, high creep resistance, low shrinkage at elevated temperatures, high specific strength and superior corrosion resistance [6]. The research shows that incorporating CNTs increases the values of some of these properties. Other research has focused on the use of CNTs in epoxy-based adhesives to hold together composite structures [7].

Other physical properties of CNTs have led to their use in sensors. They have large surface area [8] and can carry the highest current density of any metal, 10^9–10^{10} A/cm^2 [9]. This is important when using them in an electrical context. Current research at NPS is investigating the use of carbon nanofibers (CNFs) for their use in supercapacitor applications [10].

Aluminum nano- and micro-particles have also been used in composite structures. Depending on the size of particle used, different mechanical properties are affected. If nano-sized particles are used, then there is an increase in the work of fracture. If micron-sized particles are used, there is a greater increase in the fracture toughness of the material [6]. Other studies have shown that the addition of micron-sized nickel particles to a mixture of epoxy with aluminum micro-particles further increases properties such as Young's Modulus and Yield Strength [11].

2. Terahertz Technology

Many materials, such as plastic, paper, and cloth, are opaque in the infrared and visible regions of the electromagnetic spectrum are transparent to THz radiation [12]. The THz range has advantages versus X-rays, when used in sensing applications, due to the fact that THz waves are non-ionizing and harmless to human tissue. This had led to the increase in the use of THz in various scanning applications.

The use of the THz range of the electromagnetic spectrum has required extensive research into the materials that are suitable for cameras and sensors. Nano-scale metal films have studied extensively to determine the characteristics required for high absorption in the THz region [13], [14]. Sensors utilizing these technologies can then be built and used in applications involving security, biological, medical, and pharmaceutical sciences.

B. THESIS OBJECTIVES

The goal of this thesis research is to build upon the knowledge of micro- and nanoparticles and THz electromagnetic waves, specifically the interaction between the two. As the use of THz electromagnetic waves for sensors increases, it is important to know what effects it will have on the materials that are subjected to this radiation. Materials such as composites that contain nanoparticles show that they provide favorable increases in strength and toughness, but what is the effect to absorption of THz waves? This can lead to unknown heating effects within the material, which over time can have an effect on the properties of the material.

By creating a series of experiments to test the response of various micro- and nanoparticles in a variety of media to THz electromagnetic waves, the reflection, transmission, and absorption characteristics will be better understood. The data obtained from those experiments will be used in the development of finite element models that accurately represent the experimental results. Those models can then be analyzed to understand the heating effects of the radiation on both the micro- and nanoparticles and the media that contain them.

THIS PAGE INTENTIONALLY LEFT BLANK

II. EXPERIMENTAL SAMPLE PREPARATION

The goal of this research was to determine the characteristics of various nanoparticles and their response to THz electromagnetic waves and to build an accurate finite element model of the composites filled with micro- and nanoparticles. In order to accomplish this, data was collected from a series of prepared samples. Many different materials were mixed with a variety of media and then were subjected to THz electromagnetic waves. This chapter details the preparation of all of the various samples and the molds used to make the samples.

A. SAMPLE PREPARATION: MOLDS USED

A variety of media were used throughout the conduct of this research to hold the variety of particles tested. The media used were a two-part epoxy, Gardner Bender liquid tape and SPR955 positive photoresist. These media were selected based on their availability in the laboratory setting at NPS, their ease of use, and there estimated response in the THz range. When the samples were prepared, a "blank" sample of each medium was made in order to determine the THz absorption characteristics of the medium without any particles in the sample.

Due to the varying characteristics for each medium, such as viscosity and drying time, different methods of sample preparation were used throughout the duration of the research. An aluminum mold was used for the epoxy samples, and silicon wafers in various states were used with the liquid tape and the photoresist samples.

1. Epoxy-Based Substrate Mold

An aluminum mold, seen in Figure 2, was used to make the epoxy based samples. The mold was 15.24 cm (6 in) in length, 5.08 cm (2 in) in width, and 1.27 cm (0.5 in) thick. There were two holes, 5.08 cm (2 in) in diameter and 2.0 mm deep drilled into the mold to form the samples. The size of two inches diameter was selected based on the size of the sample tray of the MappIR Accessory of the Fourier Transform Infrared Spectroscopy (FTIR), which will be discussed later in this thesis. A small hole was

drilled in the center of each mold to allow high pressure air behind the sample in order to help remove it from the mold when it had dried. The NPS machine shop built the mold for the research.

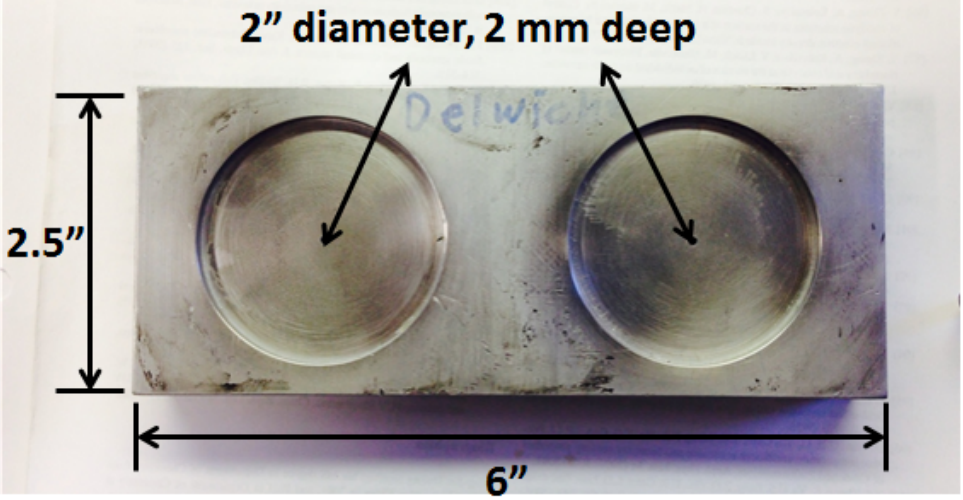

Figure 2 Aluminum Mold Used For Epoxy Based Samples

Various methods were attempted in order to determine the best one to remove the epoxy-based samples. Three different sample release conditions of the mold were used when attempting to remove the samples. The first method consisted of using multiple coats of an epoxy-release wax within the holes of the mold. The wax used was Meguiar’s Mirror Glaze 88 Universal Mold Release Wax. The second method consisted of using aircraft flash tape. This tape is used when making composite parts for aircraft to form clean edges on the part being made. The third method consisted of using the flash tape coated with the release wax.

In addition to the mold release conditions, a combination of high pressure air and heat were used when trying to remove all of the samples. Initially the mold was heated with a propane torch in order to release the sample. This method was not ultimately used for all of the samples analyzed in the FTIR as the heat may have changed some of the physical properties of the epoxy-based samples. The best method to remove the samples

was to coat the mold with at least six coats of release wax, allow the sample to dry overnight, and the use high pressure air to remove the sample.

2. Silicon Wafer Mold Used with Photoresist Solution

A mold was constructed for media that start out as a fluid and then dry into a solid. In our case, this fluid was SPR955 positive photoresist. A 300 μm thick silicon wafer was used a base. A separate silicon wafer was cleaved into smaller pieces such that two windows were formed. These windows served as the areas to put the materials to be tested. The windows were approximately 2.4 cm by 3.4 cm, and 2.1 cm by 3.5 cm. The exact size of the windows was not a major concern. The windows needed to be sufficiently large to have a sample that could easily be analyzed in the FTIR. The cleaved pieces were attached to the silicon wafer base using Scotch tape. The mold, with SPR samples in it, is in Figure 3. The separate windows keep the photoresist in a single area while it dries. Unlike the aluminum epoxy mold, this mold is a one-time use mold.

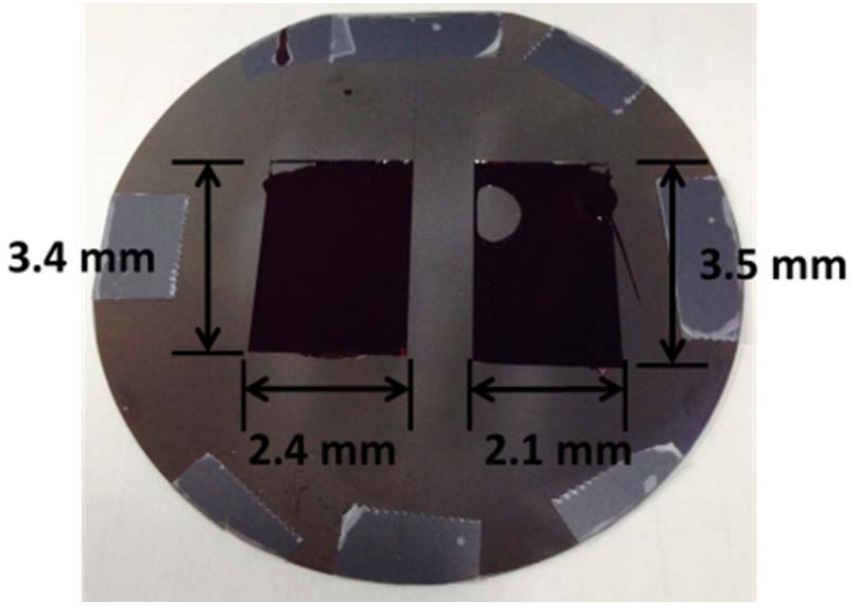

Figure 3 Silicon Wafer Mold, with Two Windows, for Photoresist Solution

3. Silicon Wafer Sandwich Mold

A reusable mold made of three silicon wafers was constructed to hold various types and sizes of nanoparticles that were not submerged in media that were liquid or solid, but in air. It was made such that it could be filled and emptied multiple times, as long as the silicon wafers were not broken.

The mold was made of one silicon wafer as a base. The next layer was made of a silicon wafer that was broken into multiple sections as to form a window, where any number of nanoparticles can be held. Two windows were built into this middle layer in order to maximize the number of measurements that could be taken. The windows are approximately 1.5 mm by 1.6 mm and 1.1 mm by 1.5 mm. Again, the size of the window only had to be large enough to be analyzed in the FTIR. The final layer is made of a complete silicon wafer. All of the silicon wafers are approximately 500 μm thick. This mold, without the top silicon wafer, is in Figure 4. All layers of this mold are held together with Scotch tape along the edges of the silicon wafers.

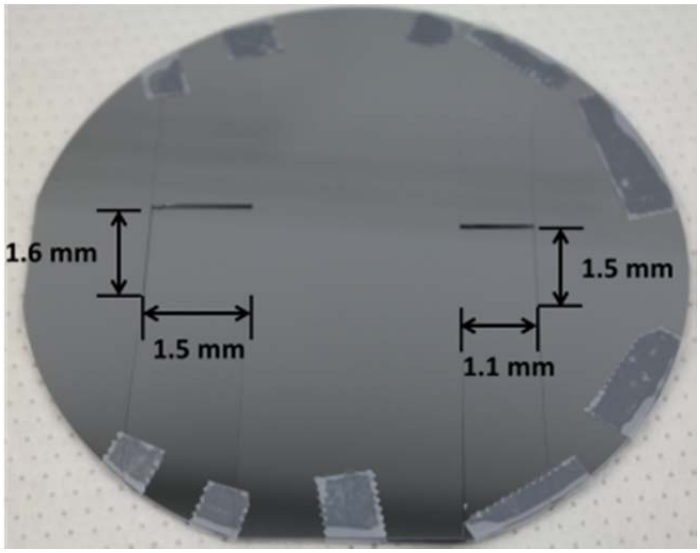

Figure 4 Silicon Sandwich Mold for Various Nano- and Microparticles

B. SAMPLE PREPARATION: MEDIA

Multiple media were used in the preparation of the samples for the experimental portion of this research. Epoxy, Gardner Bender Liquid Tape, SPR955 positive

photoresist, and air were all used as media to hold the various micro- and nanoparticles, and they are described in the following section.

1. Epoxy as a Medium

Epoxy was used as a medium for carbon nanotubes, as well as nickel microparticles. The epoxy used was a two-part epoxy made by Pro-Set. The components of the epoxy were M1002 Resin and 226 Hardener. This particular epoxy was selected as a candidate for this research based on its availability in the laboratory setting at NPS, its use in other research projects at NPS, and its ease of use.

The ratio of the resin to the hardener was three parts resin to one part hardener. For the aluminum mold discussed previously, approximately 18 mL of resin mixed with 6 mL of hardener was used to fill both of the holes in the mold. The mold was filled so that the epoxy and the epoxy with nanotubes/microparticles combination was level with the top of the mold. The samples were left to air dry overnight. Multiple samples made only of epoxy were produced to use as control samples when analyzed with the FTIR.

Multiwall CNTs were used in the epoxy substrate. The characteristics of the CNTs can be seen in Table 1. They were mixed with the epoxy in concentrations of 0.1%, 1.0%, 4.0%, and 10.0% by weight, seen in Figure 5. These weight percentages were selected based on discussions with other thesis research being conducted at the time. Additionally, the amount of CNTs increased in small increments to see what changes in absorption, if any, would be seen by varying the percentages. As the percentage of CNTs increased to 10.0%, the epoxy mixture became more difficult to mix and did not dry as smoothly as the samples that contained less CNTs.

Table 1 Multiwall CNTs Characteristics Used in Epoxy Samples

Outer Diameter	**20–40 nm**
Length	10–30 μm
Purity	>95% wt
Ash	<1.5% wt

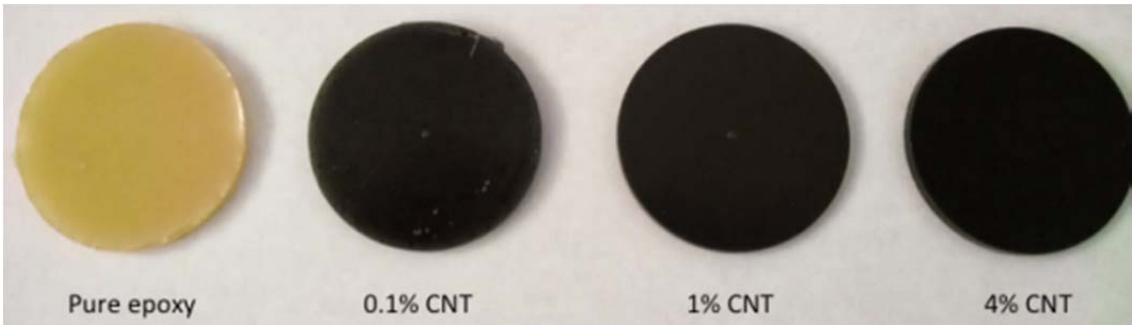

Figure 5 Epoxy-Based Samples with Various Percentages of CNTs

Nickel microparticles were also used with epoxy as a medium. The nickel nanoparticles were listed to be a nominal size of 5 μm in diameter. A Zeiss scanning electron microscope (SEM) image of the nickel powder was taken. Figure 6 shows that the particles were not all 5 μm in diameter, and in fact many of them are much smaller than 5 μm.

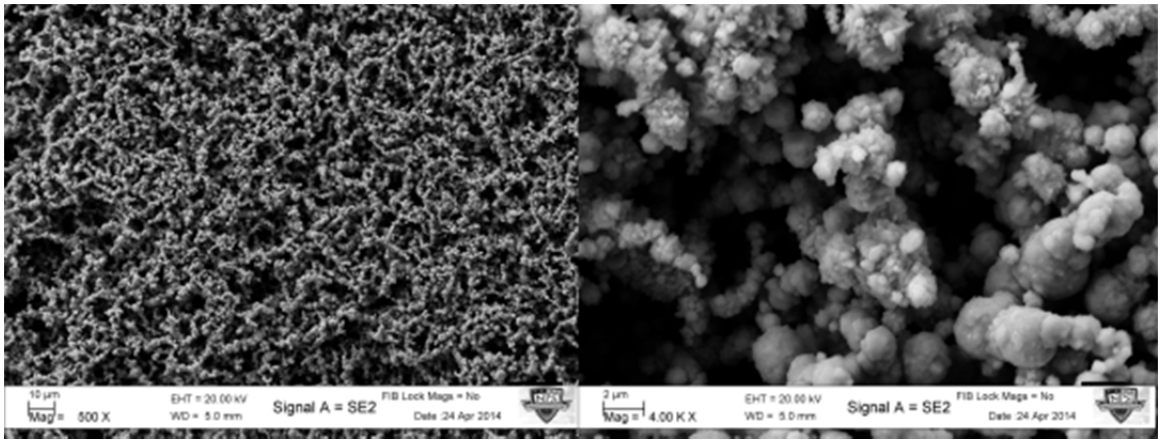

(a) (b)

Figure 6 SEM Images of Nickel Powder with Nominal 5 μm Diameter Spheres at (a) 500x Magnification and (b) 4000x Magnification

The nickel particles were mixed with the epoxy, maintaining the three to one ratio of resin to hardener. A 4.0% concentration, by weight, of nickel nanoparticles was added to the epoxy and the sample can be seen in Figure 7.

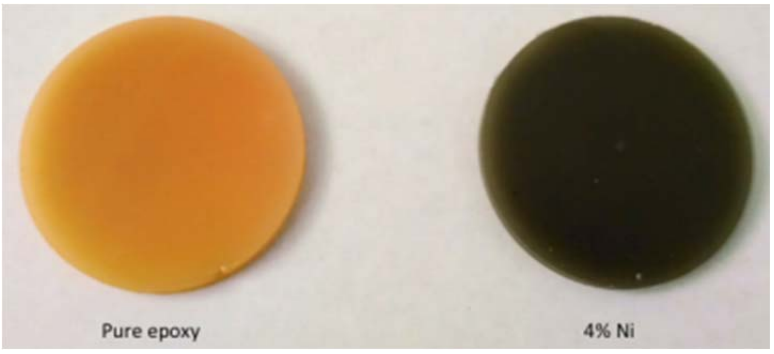

Figure 7 Epoxy-Based Samples with Nickel 5 μm Diameter Nanoparticles

2. Liquid Tape as a Medium with a Silicon Wafer as a Substrate

A substance known as liquid tape was selected as a medium to suspend the microparticles. Liquid Tape is a product produced by Gardner Bender. It is an extremely viscous material typically used to insulate and splice electrical wires. When the liquid tape dries, it becomes a solid. This material was selected in an effort to have a homogenous mixture of nanoparticles throughout its thickness. The liquid tape's response to THz electromagnetic waves was unknown when it was selected. It was believed that the metal nanoparticles would not cluster in the bottom of the mixture since the liquid tape dried quickly.

A control wafer using only liquid tape was made. The liquid tape was applied with a pipette to a 300 μm thick, four inch silicon wafer on a spin coater. The liquid tape dried very quickly, but using the spin coater, it covered a majority of the surface of the wafer as seen in Figure 8. As expected, it dried quickly and was selected as a candidate to add the aluminum nanoparticles.

Figure 8 Liquid Tape Applied with a Spin Coater Onto a 300 μm Thick, 10.16 cm (4 in) Diameter Silicon Wafer

The liquid tape was mixed with 20 μm diameter aluminum nanoparticles, with a concentration of 20% by weight. An SEM image, Figure 9, of the aluminum powder was taken to verify the diameters of the aluminum spheres. The liquid tape, with the aluminum nanoparticles, was then applied to a 300 μm thick silicon wafer using a spin coater. The silicon wafer was selected as a substrate so that the liquid tape and aluminum mixture would have flat surface to adhere to.

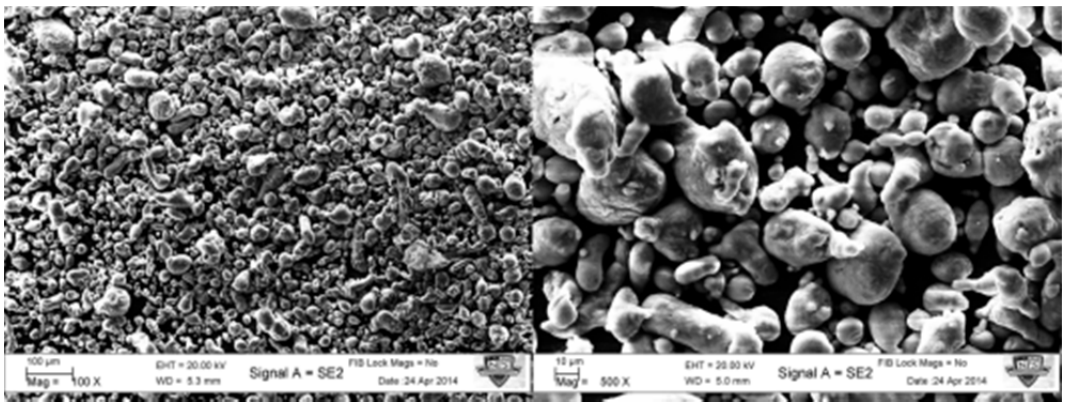

(a) (b)

Figure 9 SEM Images of Aluminum Power with Nominal 20 μm Spheres at (a) 100x and (b) 500x Magnification

Using liquid tape was difficult due to its high viscosity, especially after contact with air. It was difficult to get a smooth surface using the spin coater because the liquid tape had a very rapid drying time, even with the addition of a solvent. The uneven spreading of the mixture can be seen in Figure 10. To further investigate the effects of the uneven spreading of the liquid tape on the silicon wafer, an SEM image of a piece of the wafer was taken. Due to the amount of nonconductive material in the liquid tape, the sample had to be sputter-coated with a small layer of platinum in order to obtain a useful SEM image of the aluminum particles suspended in the liquid tape, seen in Figure 11. It can be seen that there was some clumping of the aluminum particles, as many of the particles seen in the SEM image are much larger than 20 μm. The clumping of the particles as well as the natural distribution of uneven sizes of the aluminum powder can have some significant effects in the absorption of THz at different frequencies.

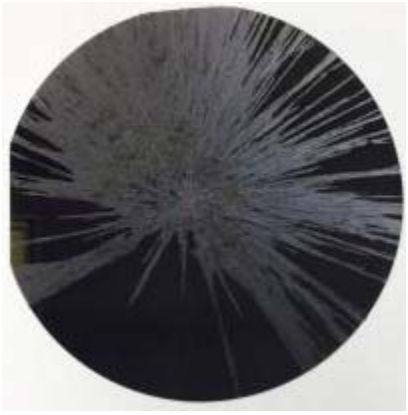

Figure 10 Liquid Tape Mixed with 20 μm Aluminum Nanoparticles, Applied with a Spin Coater, on a 300 μm Silicon Wafer

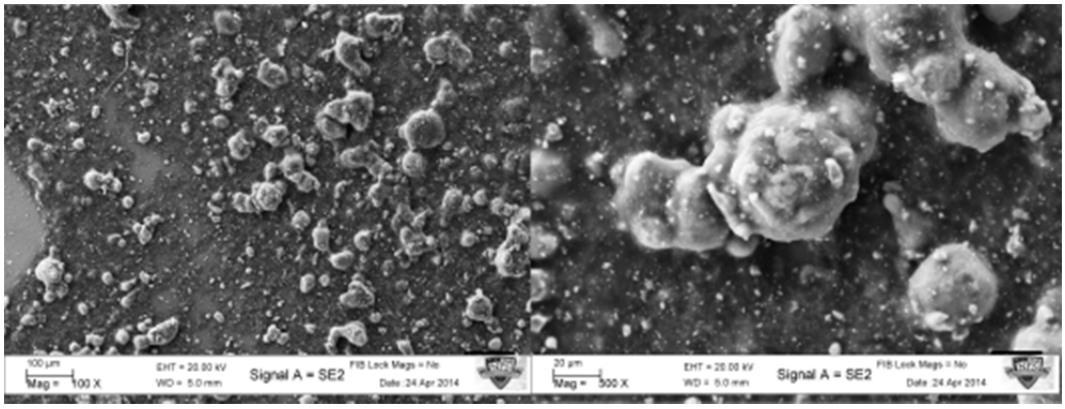

(a) (b)

Figure 11 SEM Images of Sputter Coated Liquid Tape Sample with Nominal 20 μm Diameter Aluminum Spheres in Liquid Tape Showing Clumping, Seen at (a) 100x and (b) 500x

3. Photoresist

SPR955 positive photoresist was selected as another medium for the microparticles. The photoresist was selected as it is fairly transparent in the THz range when applied in a thin film. The viscosity of the photoresist is such that particles are easily mixed into the solution. The 20 μm diameter aluminum spheres, discussed previously, were mixed into the photoresist. The photoresist was put into the silicon wafer mold, previously discussed, designed to be used for this purpose. After the photoresist was applied to the mold, it was put onto a 100 degree C hotplate to dry for approximately 10 minutes. The mold was set up such that one window was for a control sample of only photoresist. The second window was for the photoresist mixed with the aluminum particles. Unfortunately, it was difficult to get an accurate measurement of the amount of aluminum particles that were added to photoresist solution due to the viscosity of the fluid and the added precaution of working within a vapor hood when working with the fluid.

4. Various Nanoparticles in Air

Various quantities of CNTs, aluminum and nickel microspheres were tested in the silicon wafer sandwich-type mold. For these experiments, the material was simply poured

into the windows formed on the silicon wafers until the window was completely filled. The mold was weighed prior to and after each type of particle was added to determine to approximate weight of material added. Table 2 lists the various nanoparticles and amounts used in this research. Figure 12 shows the sandwich mold when it was filled with the aluminum and the nickel particles.

Table 2 Mass and Types of Particles Used in Silicon Wafer Sandwich Mold

Material	Mass Used (grams)
Multi-Walled CNTs	0.0394
5 µm diameter Nickel Spheres	0.0504
20 µm diameter Aluminum Spheres	0.1305

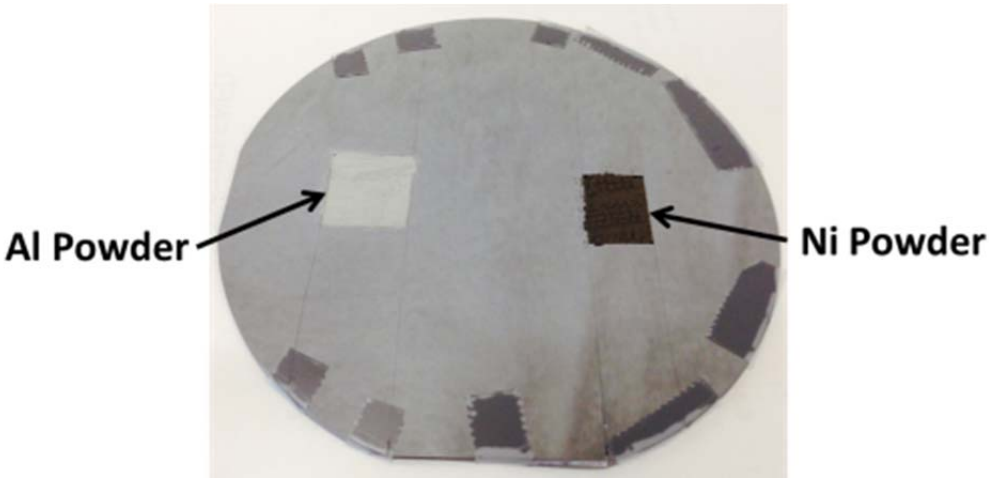

Figure 12 500 µm Thick Silicon Wafer Mold with 20 µm Aluminum Powder and 5 µm Nickel Powder

THIS PAGE INTENTIONALLY LEFT BLANK

III. EXPERIMENTAL RESULTS AND ANALYSIS

All samples were analyzed using the Thermo Scientific Nexus 870 FTIR with a Pike Technologies MappIR Automated Semi-Conductor Wafer Accessory and a standard desktop personal computer. All of the experimental results were analyzed from 5 THz to 18 THz. The results were used to build and fine tune the COMSOL models of the various samples.

A. FTIR OPERATION

In order to analyze the response of the particles in various media to THz electromagnetic waves, an FTIR, seen in Figure 13, was utilized. The device consists of a Michelson interferometer that has a mirror attached to a moving arm. The moving arm produces periodic oscillations in amplitude which changes the frequency based on the wavelength of radiation and the velocity of the moving mirror. There is a thermal detector within the FTIR that measures the frequency data and performs a Fourier Transform on the data. This process is performed across the whole spectrum of concern, which for the purpose of this research consists of wavelengths between 16.7 μm and 60 μm.

Figure 13 Thermo Scientific Nexus 870 FTIR Spectrometer

The FTIR available for use in the NPS SRL contains a globar source, consisting of a hot SiC filament, and a Deutrated Triglycine Sulfate (DTGS) pyroelectric detector with a polyethelene window. This combination of source and detector is recommended by the manufacturer for measurements in the far infrared spectrum, between 700 cm^{-1} to 20 cm^{-1} [15], which equates to 0.6 THz to approximately 21 THz. This setup is optimized for the spectrum, 5 THz to 18 THz, of concern for this research.

The Nicolet 870 is fitted with a Pike Technologies MappIR Automated Semi-Conductor Wafer Accessory. The MappIR Accessory allows the automated analysis of multiple points on a standard 4-inch silicon wafer or the 2-inch epoxy samples utilized in this research. The MappIR Accessory uses AutoPro5 software, seen in Figure 14, to control the rotation and movement of the sample. The required scanning pattern is programmed within AutoPro5 by the user. The sample tray can rotate 360 degrees and moves the sample to the positions programmed by the user using a radius and an angle of rotation from the starting position.

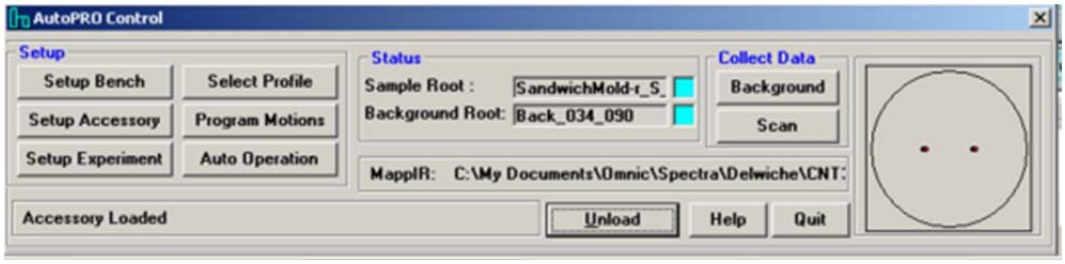

Figure 14 AutoPro5 Interface

The FTIR uses the OMNIC program for the actual spectral analysis and data collection of a sample. The OMNIC program is also used to perform the alignment of the laser after switching modes between reflection or transmission.

The FTIR has two modes of operation. One measures the transmittance of a sample and the other measures the reflectance of the material. The absorption, which is the ultimate concern throughout the course of this research, is a calculated value where Equation (1) is used.

$$\%Absorption = 100 - \%Reflectance - \%Transmittance \quad (1)$$

Changing the mode of operation is done on the MappIR Accessory. The configuration can be seen in Figure 15. Prior to each data collection run, whether it is to record reflectance or transmittance, an alignment check and background collection is required. The alignment verifies the laser's signal prior to operation.

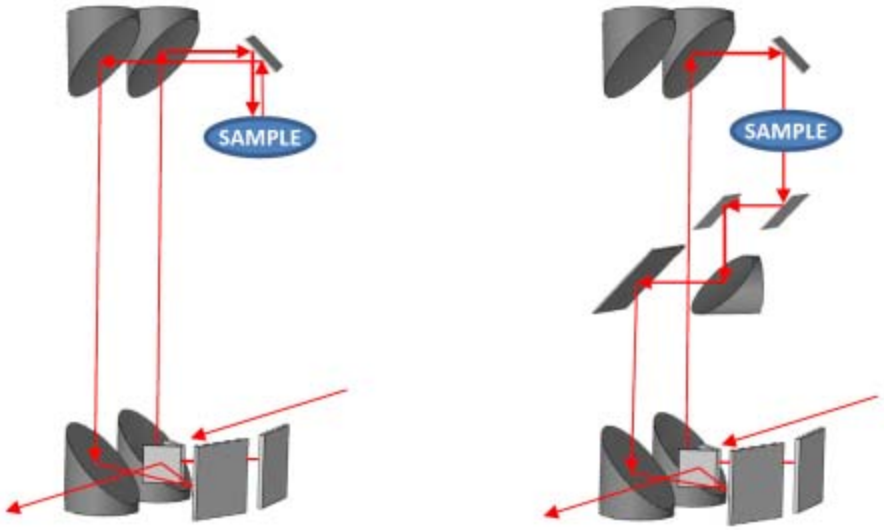

(a) (b)

Figure 15 (a) FTIR set up to measure reflection, from [16]
(b) FTIR set up to measure transmission, from [16]

The background check procedure varies based on whether the FTIR is set up to measure reflectance or transmittance. The background check is critical to the proper operation of the FTIR as it measures the 100% signal value. For a reflective background check, a silicon wafer coated with a thin film of gold is loaded into the FTIR. The gold-coated silicon wafer acts as a perfect mirror that has close to 100% reflection in the THz range. For the transmittance background check, the FTIR is not loaded with a sample or a mirror and is run empty.

All samples were analyzed from approximately 1.50 THz to 18 THz. The data obtained from 1.50 THz to 5.00 THz is not reliable due to being near the edge of the beam frequency range with a very weak signal, resulting in a large amount of noise in this range. Therefore, this range was omitted from all results.

Samples that used the silicon wafers as substrates also encountered a phenomenon known as multiple-beam interference in a parallel plate, or the Fabry-Perot effect, seen in Figure 16. An incoming wave of amplitude, E_o, and at an angle θ reaches the first surface of the silicon wafer. The silicon wafer has reflection and transmission coefficients of r and t, respectively, and internal reflection and transmission coefficients of r' and t', respectively. A portion of the wave reflects off of the surface of the wafer back toward the source with an amplitude of rE_o. The rest of the wave passes through to the back side of the wafer. Here a portion of the wave reflects back into the wafer, with an amplitude of $tr'E_o$, and a portion leaves the wafer with an amplitude of $tt'E_o$. The portion of the wave that reflects within the wafer, having an amplitude of $tr'E_o$, reaches the front side of the wafer and part of it reflects back into the wafer and part of it passes back through the front of the wafer. This series of waves leads to constructive and destructive interference patterns when the waves are recorded after passing through the wafer.

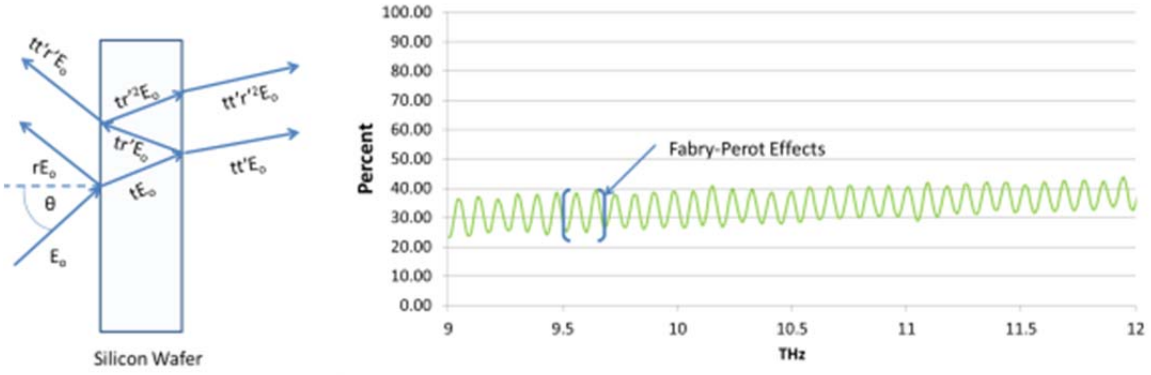

Figure 16 Multiple-Beam Interference Pattern (Fabry-Perot Effect) Due to Constructive and Destructive Interference, after [17]

Since the Fabry-Perot effect makes it difficult to discern absorption of the analyzed film from the effects of the substrate, a program was written and run in MATLAB to determine the local maximum on the experimental absorption results. The local maximum are then plotted and displayed for all samples that have silicon wafers as substrates.

B. RESULTS

Various combinations of the previously described media and micro- and nanoparticles were tested in the FTIR. Those results are contained in the following section.

1. Epoxy as a Medium

The 2″ diameter, 2 mm thick epoxy-only samples were analyzed in the FTIR. The reflectance and transmittance were measured at three points on the sample, seen in Figure 17. The sample points were the center of the sample and 12 mm from the center of the sample at the 12 o'clock and 6 o'clock positions. All three points had similar characteristics. Of note is the fact that all three points absorb 90% to 100% of the incoming THz radiation between 3 and 18 THz. These results are in Figure 18. The low transmission by the epoxy is likely the cause of some noise in the signal which contributes to the "unclean" nature of the absorption results for all samples with epoxy.

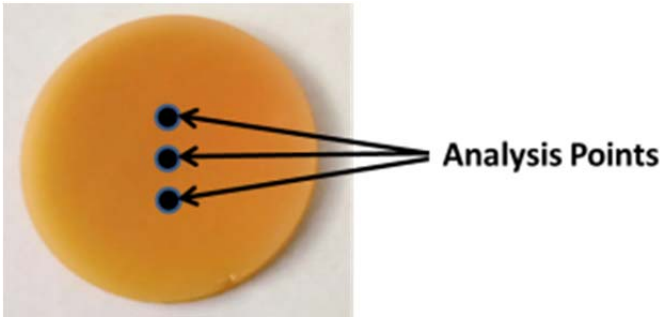

Figure 17 Epoxy Only Sample Data Collection Points

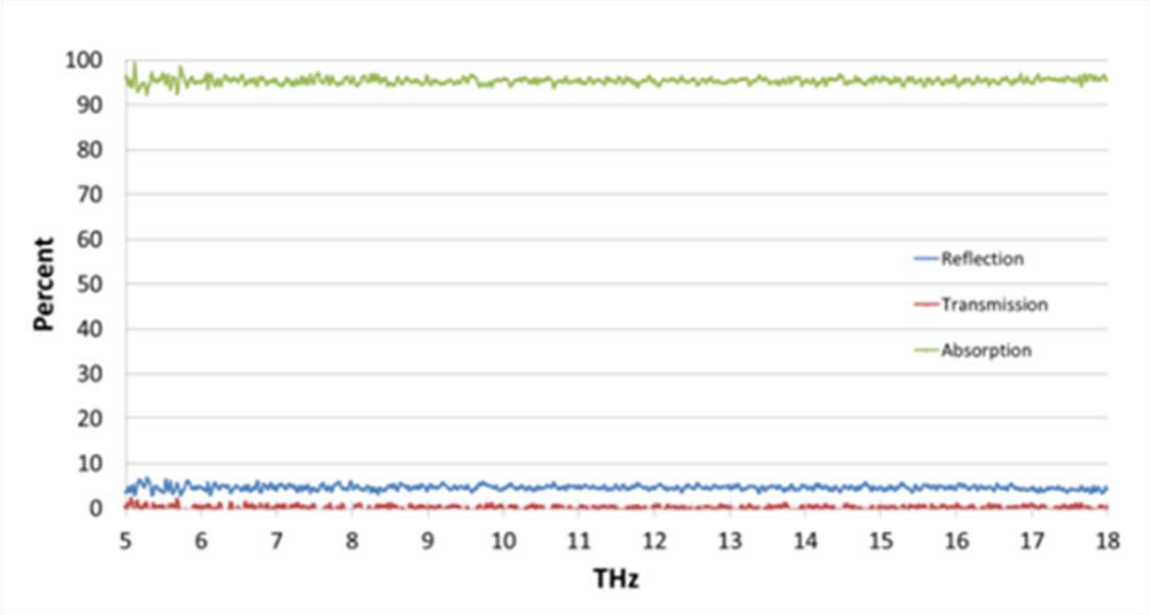

Figure 18 Experimentally Obtained Reflection, Transmission and Absorption Values of 2mm Thick Epoxy-Only Sample

All epoxy samples with CNTs were analyzed in the FTIR. Due to the similarities in the results only the epoxy sample with 10% CNTs (by weight) is discussed in this manuscript. The sample was analyzed at two points, one at the center of the sample and one 4 mm from the center. The absorption of this sample was close to 99% as seen in Figure 19.

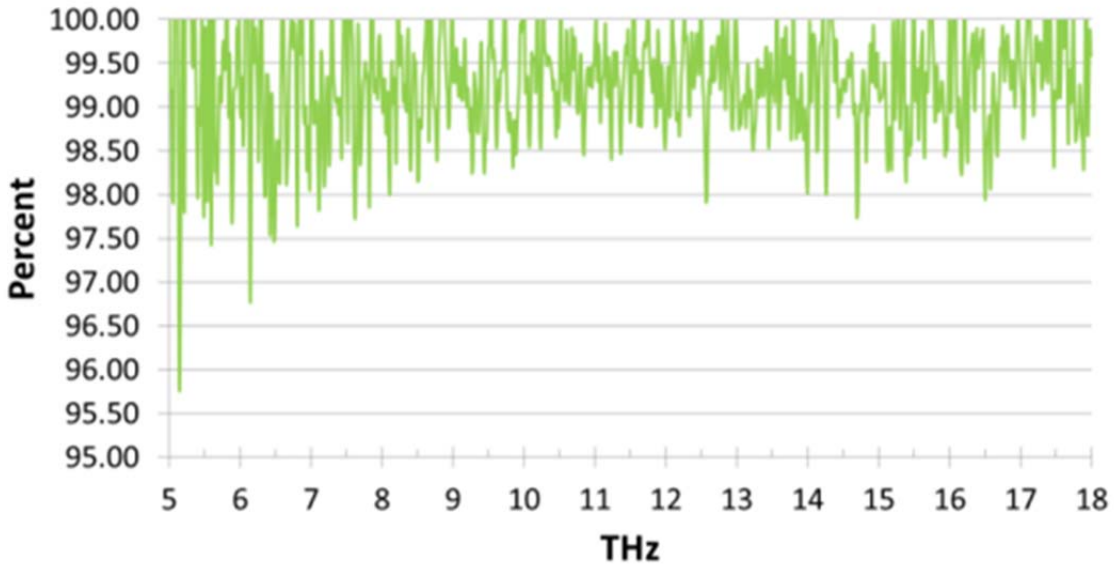

Figure 19 Absorption of THz Radiation in Epoxy with 10% CNTs

The absorption values obtained at each frequency value were averaged for the epoxy-only sample and the epoxy-based sample containing 10% CNTs. The averaged values of absorption for the epoxy-only sample were then subtracted from the averaged absorption of the epoxy with 10% CNTs sample. The results are contained in Figure 20. A simple linear, least squared average was performed on the results in the graph and it was found that the CNTs absorb approximately 4% of the THz radiation between 5 THz and 18 THz. This is a very small percentage of the incoming radiation. This small number, make it difficult to truly see the actual absorption due to the CNTs.

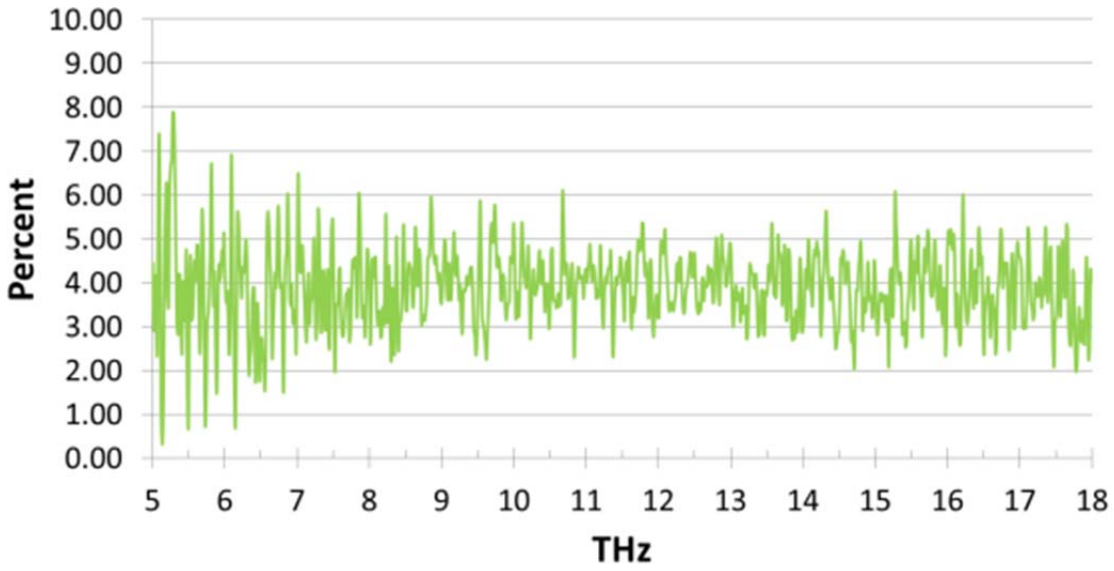

Figure 20 Absorption Due Only to CNTs

The sample made with epoxy and 4% (by weight) nickel particles was also tested in the FTIR. The results, in Figure 21, were similar to the epoxy with 10% CNTs. Approximately 94% of the THz radiation was absorbed by the sample. Again this is due to the strong absorption characteristics of the epoxy in the THz range of the spectrum. The absorption of the nickel particles alone was calculated by subtracting the absorption of the epoxy-only sample from the sample with nickel particles, and is in Figure 21. The absorption by the nickel particles is less than the absorption by the CNTs.

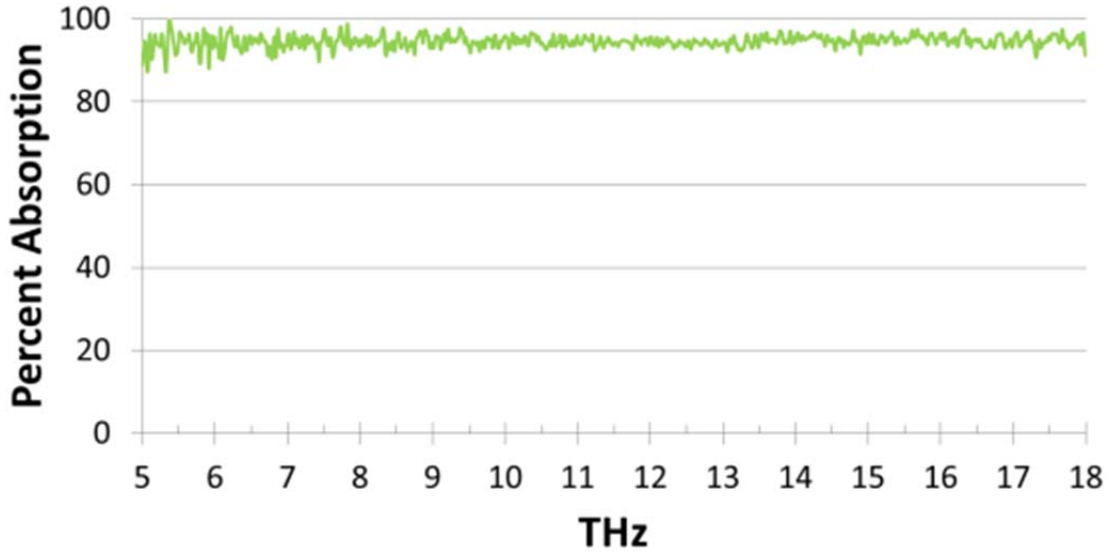

Figure 21 Absorption Characteristics of 4% (by Weight), 5 μm Diameter Nickel Spheres in Epoxy

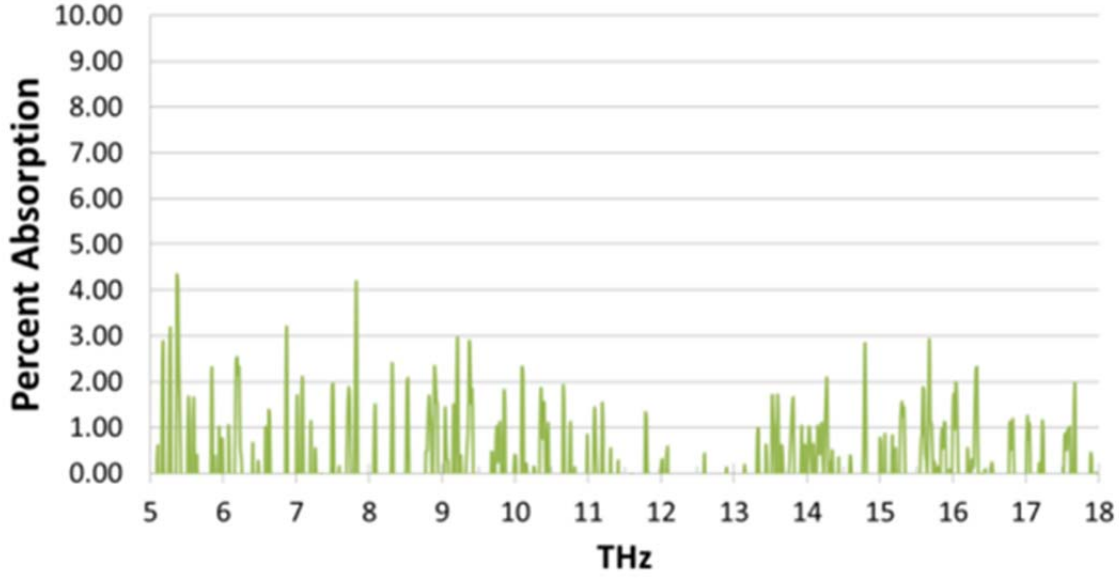

Figure 22 Absorption Due Only to 5 μm Nickel Particles

Overall, the results from both the CNTs and nickel particles in epoxy show that epoxy exhibits strong absorption in the THz range of the spectrum when the thickness is approximately 2 mm. Due to this fact, it is not the best medium to use when testing the absorption characteristics of the various nanoparticles.

2. Liquid Tape as a Medium

As with the epoxy-based samples, all of the samples using the liquid tape as a medium were analyzed using the FTIR to obtain reflection and transmission characteristics. For the sample containing only liquid tape on a silicon wafer substrate, three sample points were selected for analysis. One sample point was in the center, with the other two points located 12 mm from the center, along the vertical centerline of the sample. The calculated absorption values at the three sample points were averaged and plotted as seen in Figure 23. There are very distinct peaks as the absorption varied dramatically throughout the range of interest.

The sample containing liquid tape mixed with 20% (by weight) aluminum particles exhibited absorption characteristics as seen in Figure 24. The calculated absorption data from Figure 23 and Figure 24 were combined in the way described in previous chapter to extract the effect due only to the aluminum particles. The combined data is captured in Figure 25.

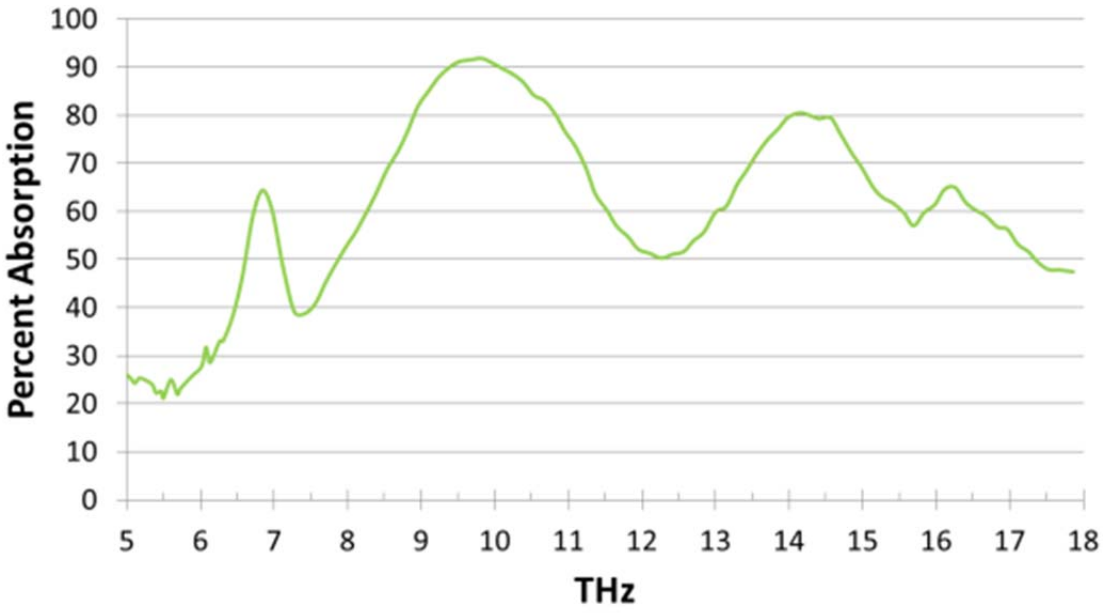

Figure 23 Absorption Characteristics of a Thin Layer of Liquid Tape on a 300 μm Silicon Wafer

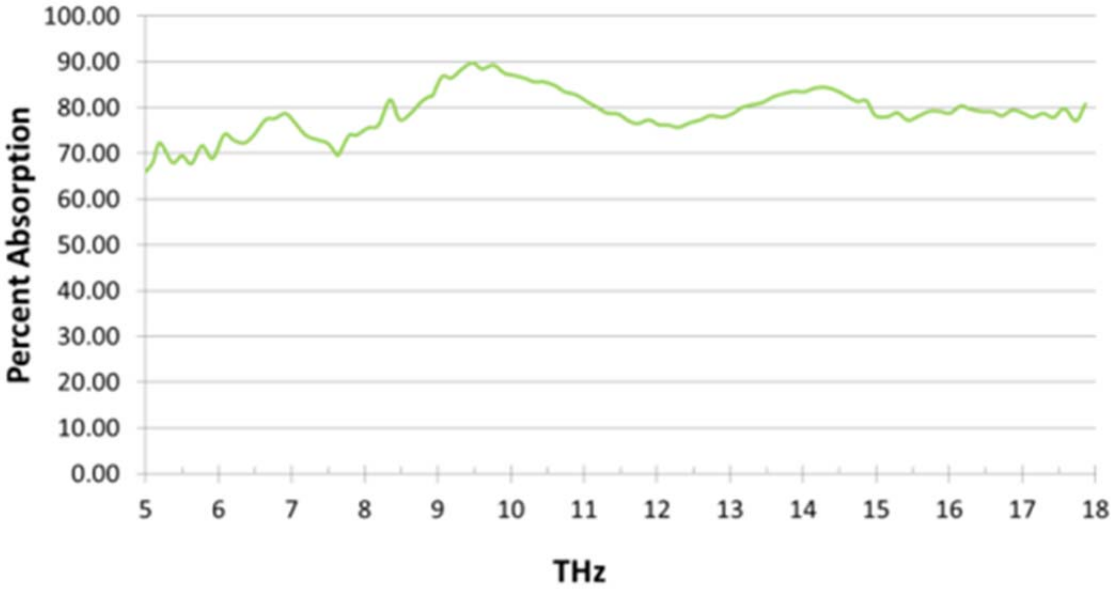

Figure 24 Absorption Characteristics of Liquid Tape with 20% Aluminum Spheres on a 300 μm Silicon Wafer

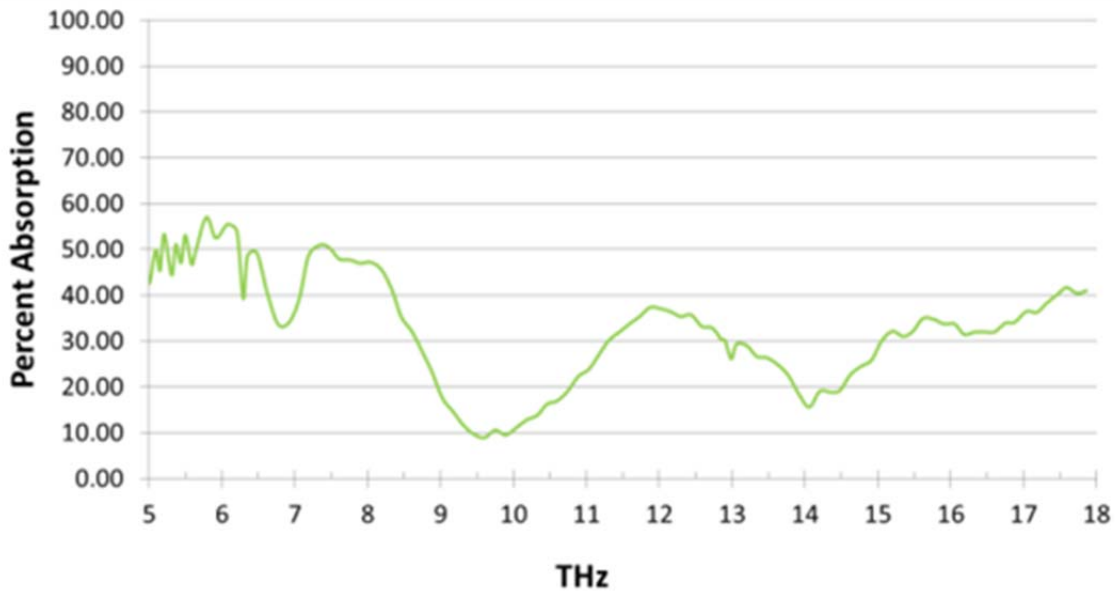

Figure 25 Absorption of Only 20 μm Aluminum Spheres

3. Photoresist as a Medium

FTIR measurements were taken on the sample prepared with the SPR955 positive photoresist as the medium. The reflection and transmission were measured at five

different points on the photoresist only window. The window that contained a mixture of photoresist and aluminum particles was measured at three different points. . The average absorption in the photoresist only sample was calculated and can be seen in Figure 26. The averaged absorption of the three points of the photoresist with aluminum nanoparticles sample is contained in Figure 27. The absorption due to the aluminum particles alone was calculated from the averaged absorption of the photoresist alone subtracted from the averaged absorption of the photoresist with aluminum particles and can be seen in Figure 28.

Again it can be seen that the absorption due to the aluminum particles alone is a very small number between 5 THz and 18 THz, and it is on the same order of magnitude as was previously seen on the samples of aluminum in epoxy samples. However, the aluminum particles in epoxy maintain a fairly consist absorption of 4% through the whole range where the aluminum in photoresist tapers off toward zero. This can be due to the random size distribution of particles in the two samples or different amounts of aluminum in each sample.

One additional issue encountered during the testing of the photoresist solution was the fact that in early testing the sample did not seem to be fully dry. As testing continued it appeared to be more dry. This can explain some of the differences seen in the absorption characteristics of the samples as the amount of water in the photoresist decreased due to evaporation.

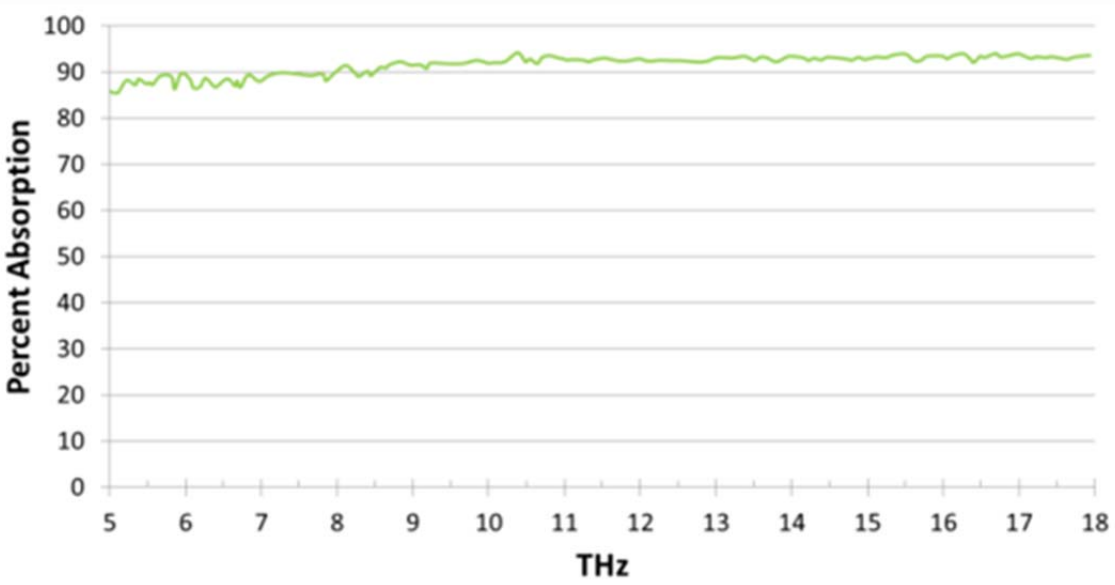

Figure 26 Averaged Absorption of Photoresist Only

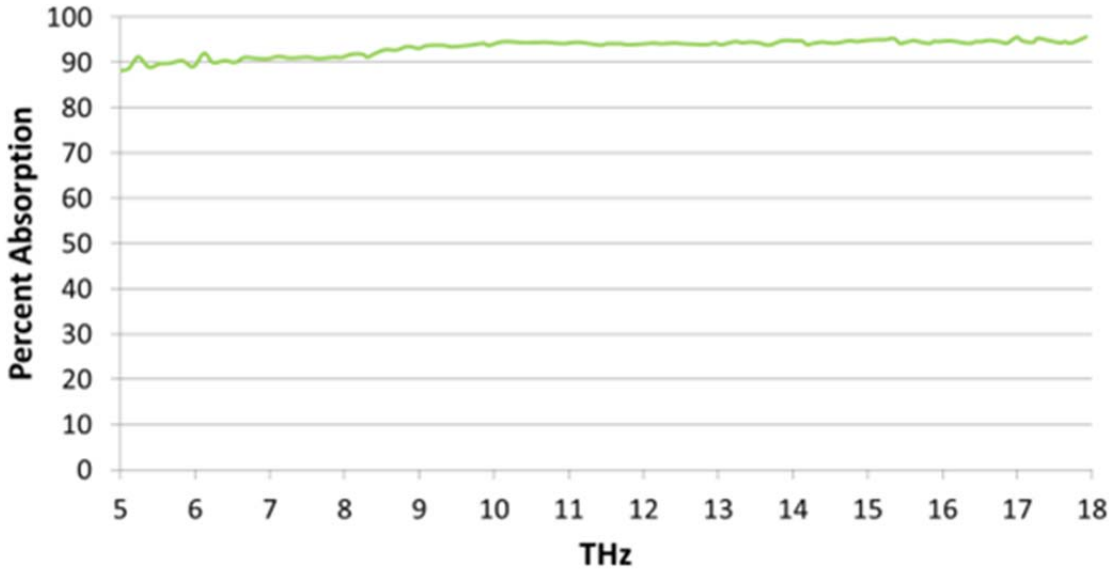

Figure 27 Averaged Absorption of Photoresist with 20 μm Aluminum Particles

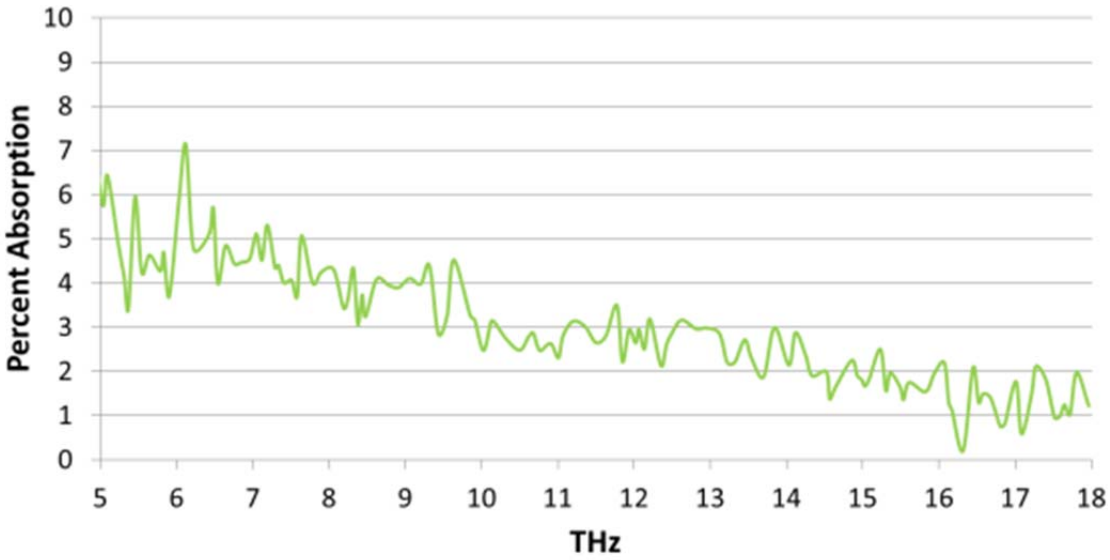

Figure 28 Averaged Absorption of 20 μm Aluminum Particles Alone

4. Various Particles in Air

The silicon wafer sandwich mold was analyzed using a variety of particles. In order to see the amount of absorption due to each type of particle, results from the absorption due to the silicon wafer and air obtained from analyzing the blank window in the sandwich mold were subtracted from the results from the mold filled with the various particles. Each window of the silicon wafer was analyzed at three different points in the center of each window. The points were in a horizontal line, spaced 2 mm apart.

The first sample analyzed was the blank window, filled only with air. The absorption values obtained at all three sample points were averaged and the results are in Figure 29. The absorption is due to two 500 μm thick silicon wafers and a 500 μm thick airspace between the wafers. The absorption ranges between 25% and 70% due to Fabry-Perot effect.

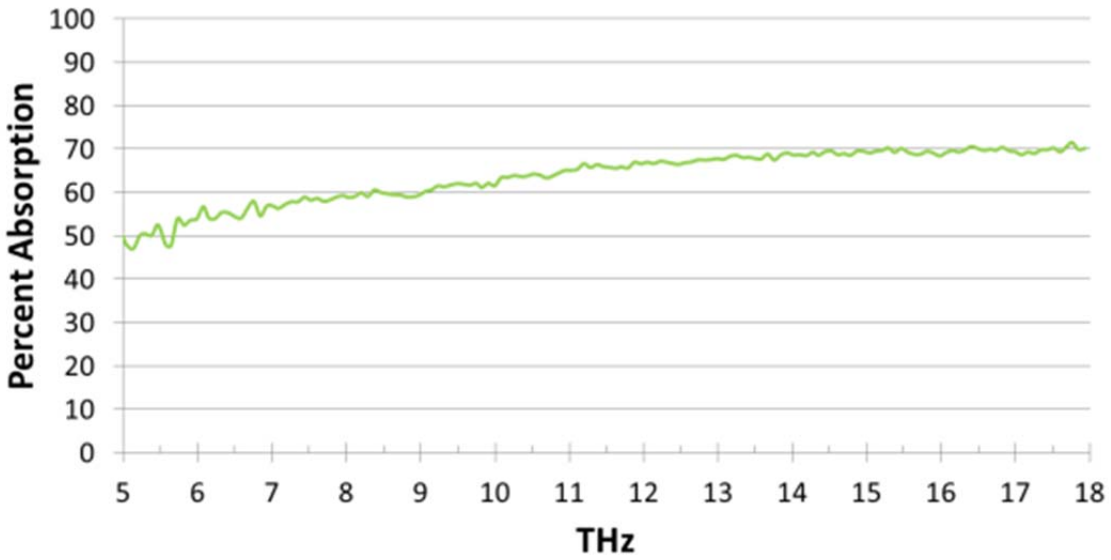

Figure 29 Absorption Characteristics of the Average of Three Sample Points on the Silicon Sandwich Mold, Blank Window

The multi-walled CNT sample was analyzed at three points and the absorption values of the three points were averaged, seen in Figure 30. Those values were then subtracted from the averaged absorption values of the blank window of the silicon sandwich mold in order to determine the absorption due to the CNTs alone.

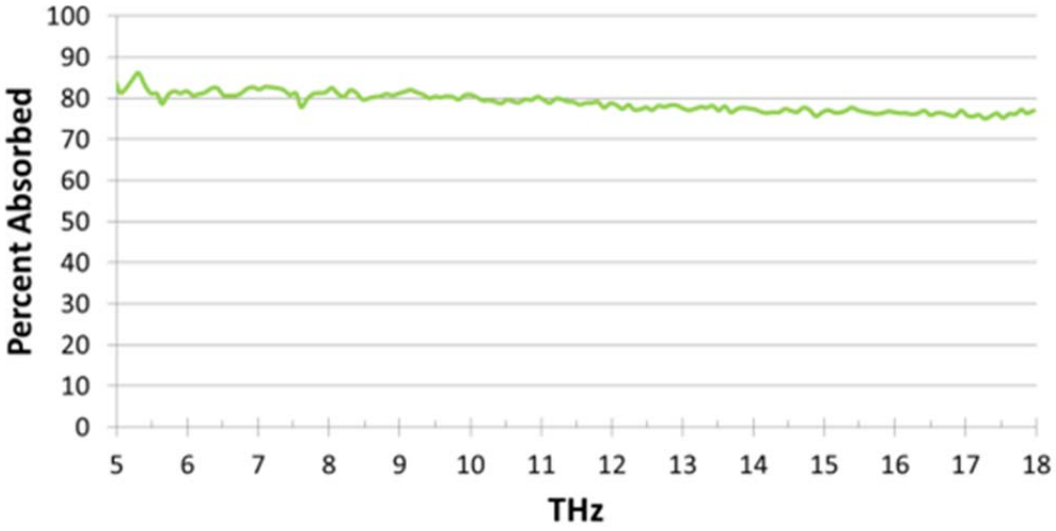

Figure 30 Averaged Absorption Characteristics of Multi-Walled CNTs in Air in the Silicon Sandwich Mold

As seen in Figure 31, the multi-walled CNTs absorb close to 35% of the incoming radiation at 5 THz but then trail off to approximately 7% close to 18 THz. This is more absorption than was seen in the 10% CNTs in epoxy sample between 5 THz and 18 THz. The general trend of the CNTs in air is also different than the CNTs in epoxy. The CNTs in epoxy maintain a fairly constant level of absorption between 5 THz and 18 THZ, where the CNTs in air had much higher absorption low in the frequency band and it decreases as it approaches 18 THZ. The difference is likely due to the difference in the density of CNTs in both instances. In the epoxy, the density of the CNTs was 0.04157 g/cm^3, where the density of CNTs in the air was 0.32833 g/cm^3. The volume density of CNTs in the sandwich mold is almost ten times greater than that of the CNTs in epoxy.

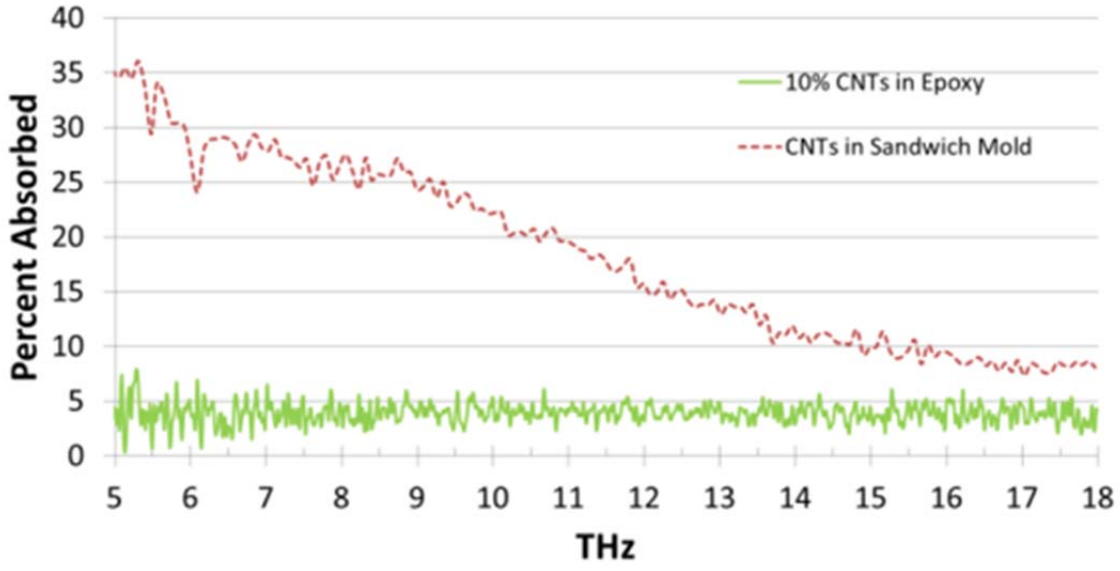

Figure 31 Averaged Absorption Due Only to Multiwall CNTs with Size Characteristics as Found in Table 1

The aluminum particles were analyzed at the same points as the multi-walled CNT sample and the results are in Figure 32. Again, the values of the blank window were subtracted from the averaged values obtained from the aluminum particle analysis. These results, as well as the aluminum particles in the liquid tape and the photoresist, are in Figure 33. Like the previous results concerning the aluminum powder, there is decreasing trend in toward zero as the THz wave goes from 5 THz to 18 THz. When the absorption

due to the aluminum particles in air is compared to the aluminum in the photoresist, the aluminum in the air absorbs more of the incoming THz wave. This result is expected, like with the CNTs, because the concentration of aluminum is much greater for the silicon wafer mold versus the aluminum in the photoresist. The aluminum particles in the liquid tape showed more absorption through the entire frequency spectrum, even though they were only mixed with a 20% by weight ratio into the liquid tape. The relatively high absorption rate between 5 THz and 8 THz could be due to the clumping of the aluminum particles seen previously in this thesis as well as presence of particles larger than 20 μm. The larger, clumped, aluminum particles absorb a greater amount of the incoming THz wave low in the spectrum of interest. Another factor in the high experimental absorption rates of the aluminum particles in liquid tape is the fact that there may be some scattering effects that are not accounted for in the experimental measurements. One assumption when using the FTIR is that the incoming wave is transmitted, reflected, or absorbed. There is not a way to measure any waves that are scattered within the FTIR.

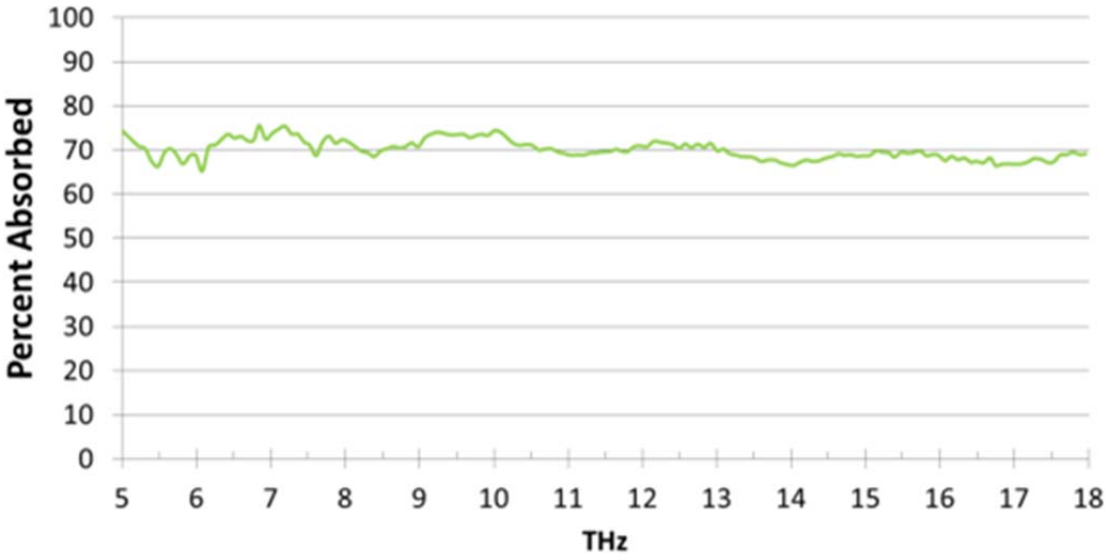

Figure 32 Absorption of 20 μm Aluminum Spheres in Air, in Silicon Wafer Sandwich Mold

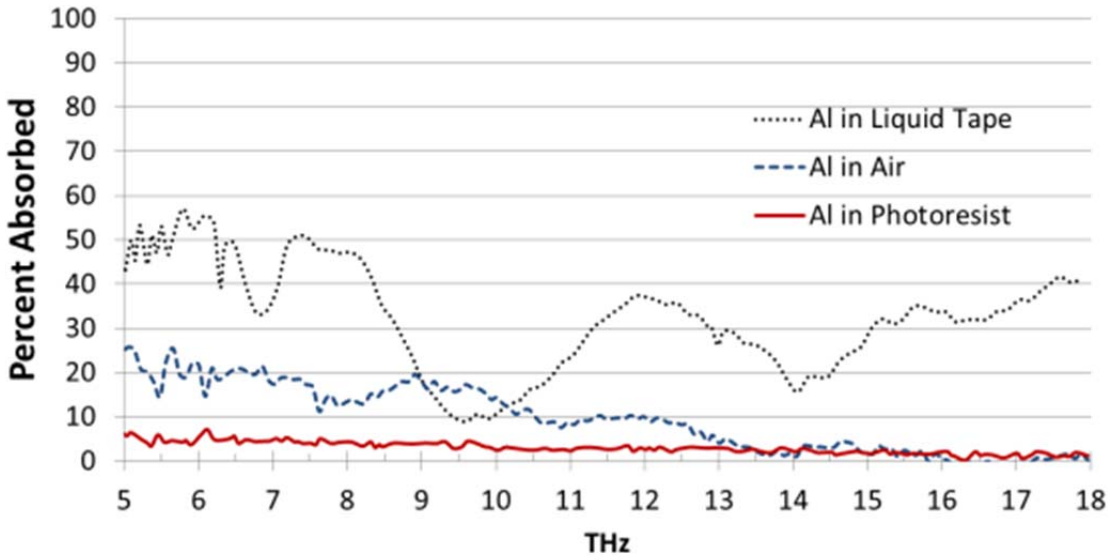

Figure 33 Absorption Due only to 20 μm Aluminum Spheres

Finally, the nickel particles were analyzed using the silicon sandwich mold and the results are in Figure 34. The same type of analysis was performed as discussed previously for CNTs and aluminum to determine the absorption due only to the nickel particles. Figure 35 shows that the nickel particles absorb less than 10% of the incoming THz wave for most of the spectrum and it decreases toward zero as the values move to 18 THz. This result is similar to the absorption characteristics of the nickel particles in epoxy. The magnitude of absorption is higher for the nickel particles in air, but like the aluminum particles, this could be due to the increased volume of nickel particles in this mold.

In general, both the nickel and aluminum particles absorb a very small percentage of the incoming THz wave and both types of particles show decreasing trends from 5 THz to 18 THz.

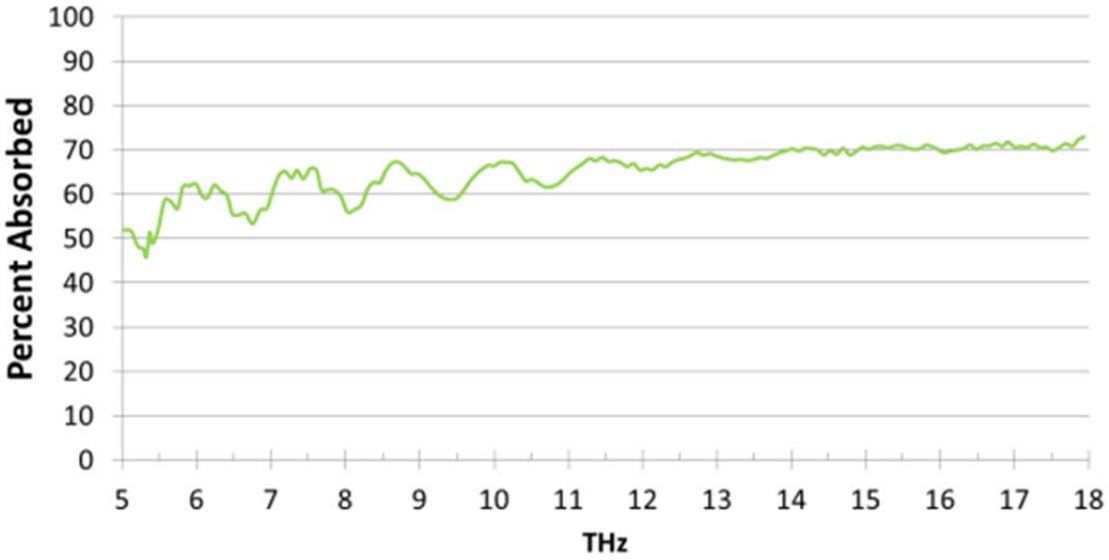

Figure 34 Average Absorption of 5 μm Nickel Spheres in Air, in Silicon Wafer Sandwich Mold

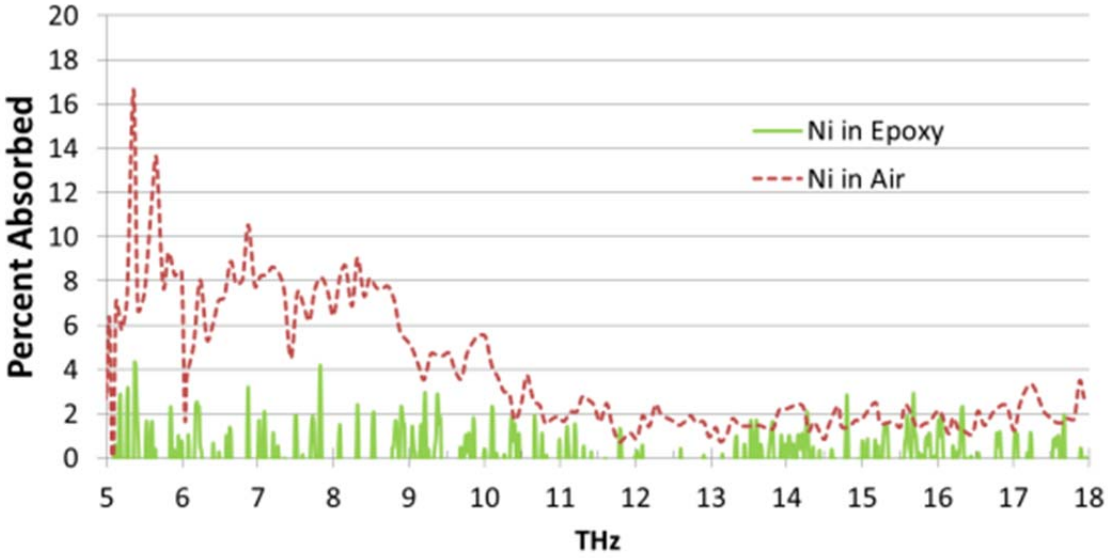

Figure 35 Average Absorption Due Only to 5 μm Nickel Spheres

C. DETERMINATION OF REFRACTIVE INDEX

Many of the materials, such as the epoxy and the photoresist, used as media throughout this research did not have readily accessible values for the real (n) and imaginary (k) components of refractive index. Additionally, both the real and imaginary

components of the refractive index are frequency-dependent at those frequencies. The refractive index values are required inputs into the COMSOL models and are needed for an accurate model simulation. The method used to determine the refractive indices takes the experimental reflection and transmission measurements and applies the Transfer Matrix Method. The basic theory is described by Pedrotti and Pedrotti in [17]. The specific method used in this research is described by Martin in [18].

In order to estimate the refractive indices of the materials used throughout this research a Thin Film Analysis Tool was used. The tool was created by Dr. Fabio Alves, a professor at NPS, and Major Michael Martin developed the tool. The tool was designed such that a graphical user interface (GUI), designed in Labview 2012, allows a user to adjust various parameters so that the reflection, transmission, and absorption curves match the experimentally derived values. The Transfer Matrix Method calculations are performed by MATLAB, so the user must have MATLAB and Labview 2012 installed on their computer for the program to run properly.

The Fabry-Perot effects did make it more difficult to precisely match the experimental and simulated data. Figure 36 shows an example of the simulated and experimental reflection, transmission, and absorption curves that were required to be matched to determine n and k. The Fabry-Perot effects are clearly visible in Figure 36. After the simulated and experimental values were matched, a plot of n and k versus frequency was created to show the frequency dependence of those values, as seen in Figure 37 and Figure 38.

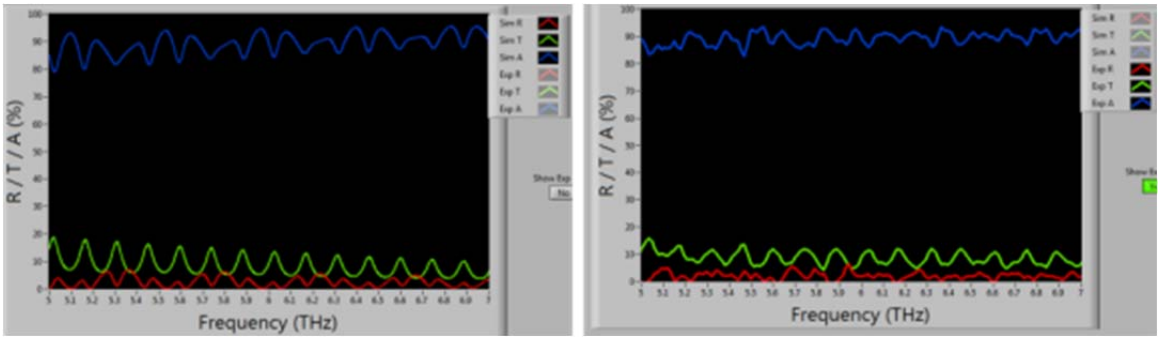

(a) (b)

Figure 36 (a) Simulated Reflection, Transmission and Absorption in Transfer Matrix Method GUI
(b) Experimental Reflection, Transmission, and Absorption in Transfer Matrix Method GUI

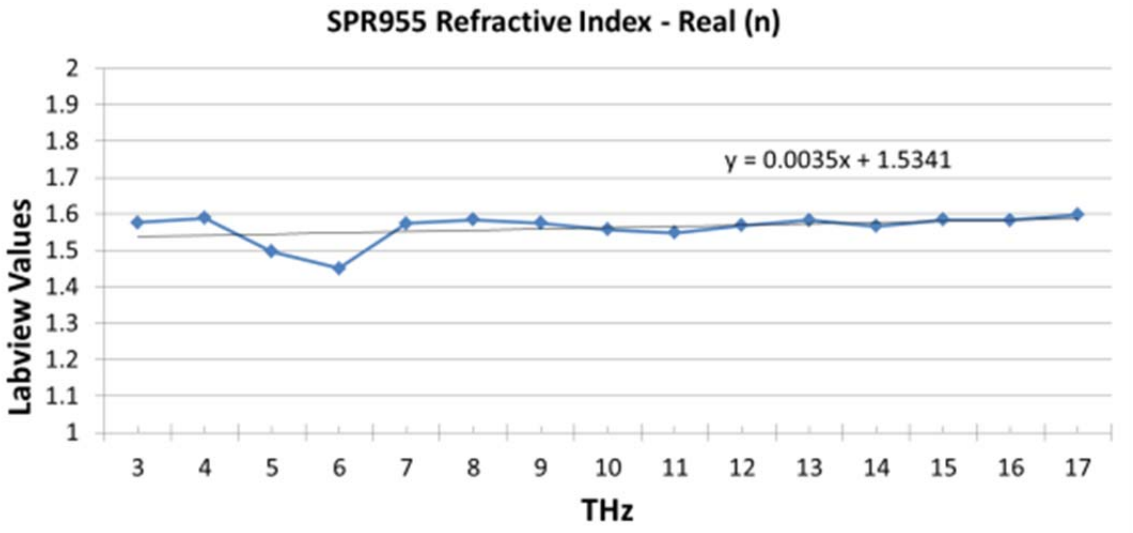

Figure 37 Thin Film Analysis Values and Linear Fit for SPR955 Real Portion of Refractive Index

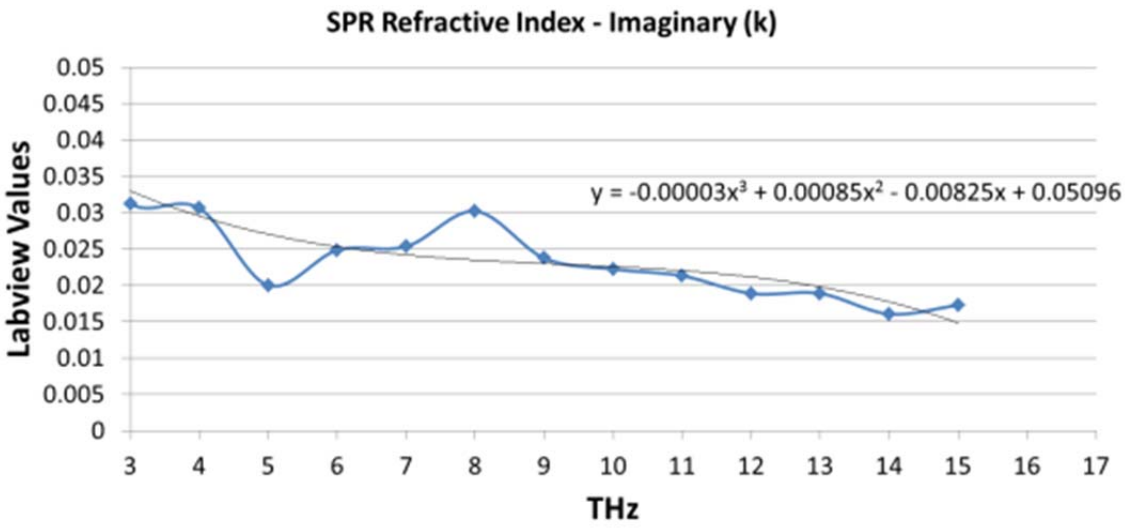

Figure 38 Thin Film Analysis Values and Second Order Polynomial Best Fit for SPR955 Imaginary Portion of Refractive Index

IV. MODELING

The software used for the modeling portion of this research was the COMSOL Multiphysics program, using the RF module to simulate electromagnetic waves. The RF module solves Maxwell's equations. COMSOL was selected due to its ability to model multiple physics interactions within a model. COMSOL has been used to support various research topics involving the THz portion of the electromagnetic spectrum at NPS.

A. COMSOL RF MODULE

COMSOL solves the series of equations known as Maxwell's equations. The equations handle some basic electromagnetic quantities. The quantities are the electric field intensity (**E**), the electric flux density (**D**), the magnetic field density (**H**), the magnetic flux density (**B**), the current density (**J**) and the electric charge density (ρ). The form of Maxwell's equations used by COMSOL can be seen in Equations (2)-(5):

$$\nabla \times \mathbf{H} = \mathbf{J} + \frac{\partial \mathbf{D}}{\partial t} \tag{2}$$

$$\nabla \times \mathbf{E} = -\frac{\partial \mathbf{B}}{\partial t} \tag{3}$$

$$\nabla \bullet \mathbf{D} = \rho \tag{4}$$

$$\nabla \bullet \mathbf{B} = 0 \tag{5}$$

Within each COMSOL model, the equations are modified in order to account for conductive or dielectric material and they rely on a series of constitutive relationships. The materials within the model that are conductive use Equation (6) as the governing equation and Equation (7) as a constitutive relationship:

$$\nabla \times \mu_r^{-1}(\nabla \times \mathbf{E}) - k_0^2(\varepsilon_r - \frac{j\sigma}{\omega\varepsilon_0})\mathbf{E} = \mathbf{0} \tag{6}$$

$$\mathbf{B} = \mu_0 \mu_r \mathbf{H} \tag{7}$$

where μ_r is the relative permeability of the material, ε_r is the relative permittivity of the material, σ is the conductivity of the material. The required inputs to COMSOL for conductive materials are μ_r, ε_r, and σ.

Materials that are a dielectric use Equations (8)-(11) for their governing and constitutive equations:

$$\nabla \times (\nabla \times \mathbf{E}) - k_0^2 \varepsilon_r \mathbf{E} = \mathbf{0} \tag{8}$$

$$\varepsilon_r = (n - ik)^2 \tag{9}$$

$$\sigma = 0 \tag{10}$$

$$\mu_r = 1 \tag{11}$$

where n is the real component of the refractive index and k is the imaginary component of the refractive index. COMSOL requires n and k as material properties for the materials that are dielectrics.

B. MODELING A SINGLE UNIT CELL

One particular topic related to this current research was a paper written by Alves et al. As part of the research for that paper the authors created a COMSOL model made up of a single unit cell of metamaterial [19]. This basic model was modified in order to better fit this research. A representative model used in this research can be seen in Figure 39. The incoming THz radiation is denoted by **k**, with the associated magnetic and electric fields, shown by **B** and **E**, respectively.

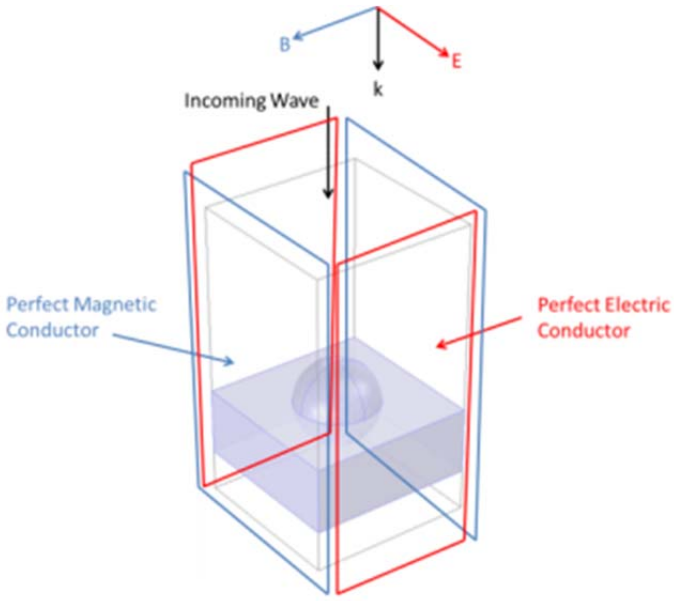

Figure 39 Schematic of 3D Finite Element Model of a Unit Cell Consisting of a Single Aluminum Sphere in Liquid Tape

The boundary conditions perpendicular to the magnetic field are Perfect Magnetic Conductors. The equation for this boundary condition is:

$$\mathbf{n} \times \mathbf{H} = \mathbf{0} \tag{12}$$

This boundary condition ensures that the tangential component of the magnetic field is zero and the surface current is zero. This allows it to be used as a symmetry type boundary which is useful in modeling a unit cell to simulate the infinitely repeating film.

Similarly, the boundary conditions perpendicular to the electric field are Perfect Electric Conductors. This equation is:

$$\mathbf{n} \times \mathbf{E} = \mathbf{0} \tag{13}$$

Again, this boundary condition ensures that the tangential component of the electric field is zero and is needed to replicate a symmetric boundary condition that simulates an infinite plane.

Above and below the unit cell are regions simulated as air. These regions are set up using a Scattering Boundary Condition with Equation (14) as the boundary conditions. On the upper portion of the model, this boundary condition will act a sink and not allow

any reflected waves to be reflected back into the model. All waves that progress all the way through the model will continue to the Scattering Boundary Condition below the unit cell where again the air acts as a sink and will not allow the waves to reflect back into the model.

$$\mathbf{n}\times(\nabla\times\mathbf{E})-jk\mathbf{n}\times(\mathbf{E}\times\mathbf{n})=-\mathbf{n}\times(\mathbf{E}_0\times(jk(\mathbf{n}-\mathbf{k}_{dir})))e^{-jk\mathbf{k}_{dir}\cdot\mathbf{r}} \tag{14}$$

In order to account for the portion of the incoming wave that is absorbed by the medium and microspheres, a volume integration of resistive heat losses is performed on the material of concern. The incoming THz wave is set at 1 W, which makes for a convenient estimation of the percentage of the power absorbed by the material of interest. This forms the basis of the models that will be used to compare to the experimentally derived results.

In an attempt to minimize the complexity of the model analyzed within COMSOL, a unit cell model was the basis for all modeling performed in support of this research. The basis for the unit cell used was the model from Alveset al., discussed previously. Various configurations of unit cells were built to see which most closely replicated the experimentally obtained results.

One important aspect of modeling in COMSOL is the generation of the mesh. The mesh size should be such that the elements are no larger than one-fifth of the incoming wavelength in size. The wavelengths analyzed in COMSOL were set up such that 5 THz to 18 THz were analyzed. This equates to wavelengths between 16.7 μm to 60 μm, thus the element lengths should be between 3.34 μm to 12 μm. As the wavelengths get smaller, the mesh will become very dense. This will add many degrees of freedom to the models. Since controlling the mesh size is an important aspect in the amount of time that it takes for each finite element model to run, a balance needs to be made as to a good size for the maximum size of the elements used in the models. The mesh density varied for each model to strike a balance between a dense enough mesh and a reasonable computation time.

1. Medium and Substrate Models

In an effort to ensure the modeling methodology used in this research was correct, simple models consisting of a small "unit cell" of various substrates and media were built and analyzed. This allowed for reasonable estimations of the real and imaginary parts of the refractive indices for the silicon wafer substrates and the various media used. A model was built for the liquid tape on a silicon wafer sample.

The model consisting of the liquid tape only sample was run with varying thicknesses of liquid tape. The range of thickness was 12 μm to 19 μm. The refractive index, both real and imaginary portions, of the liquid tape was determined by matching the experimentally obtained liquid tape data to simulated values in the Thin Film Analysis. The estimated values used for the refractive index of the liquid tape were n= 2.84343 and k=0.2121.

The results of varying the liquid tape thickness as well as the experimental data are plotted in Figure 40. Each micron change in thickness has a significant effect on the position of the peak absorption values. The actual thickness of the layer of liquid tape on the silicon wafer was measured using the KLA Tencor D-120 Profilometer. The average value obtained equated to a layer 13 μm thick. This number was based on the average of three measurements, all of which varied significantly. Based on the results from COMSOL, it would appear that the peaks, seen in Figure 41, most closely align when the thickness of the liquid tape is 16 μm. This value was used for the model containing one aluminum sphere in liquid tape, to be discussed later. The results also show that the values for both the real and imaginary parts of the refractive index are not 100% accurate and require further refinement.

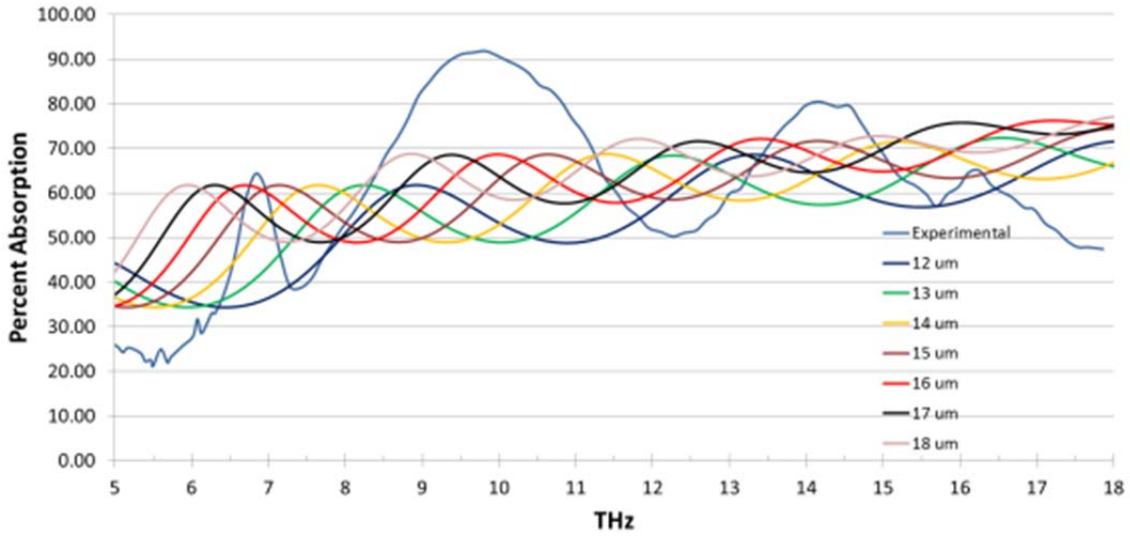

Figure 40 Absorption Characteristics of a Thin Layer of Liquid Tape with Thicknesses Varying from 12 μm to 18 μm

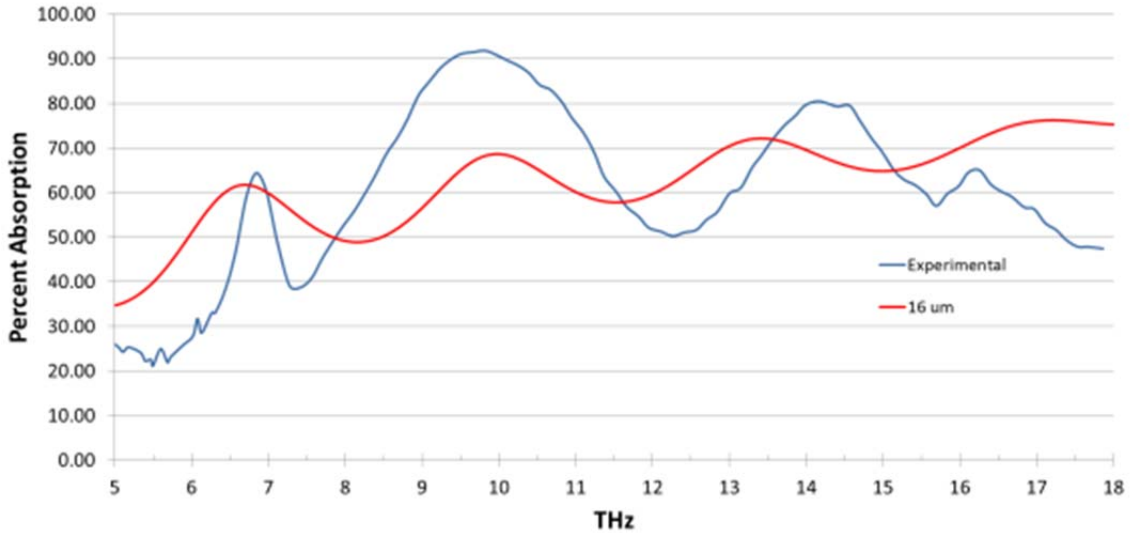

Figure 41 Absorption Characteristics of a 16 μm Layer of Liquid Tape

2. A Single Microsphere in a Thin Medium

The simplest model built was a single microsphere in a thin medium. This model contained one aluminum sphere, 20 μm in diameter, on 16 μm of liquid tape. The space above the sphere is air, as well as the space below. The modified version, based on the liquid tape model mentioned previously, has one aluminum sphere partially submerged in

the liquid tape. Both models are in Figure 42. The thickness of the liquid tape remained at 16 μm. The results for both models are plotted with the experimentally obtained data in Figure 43. Both of the COMSOL models have absorption values well below the experimentally derived values. This is likely due to inaccurate values for the refractive indices. Another source of difference between the experimental and the results from the model could be due to the scattering effects possible in the experimental results. The overall shape appears to be close to the experimentally derived values, so using a value of 16 μm is likely close to the actual value of the liquid tape thickness.

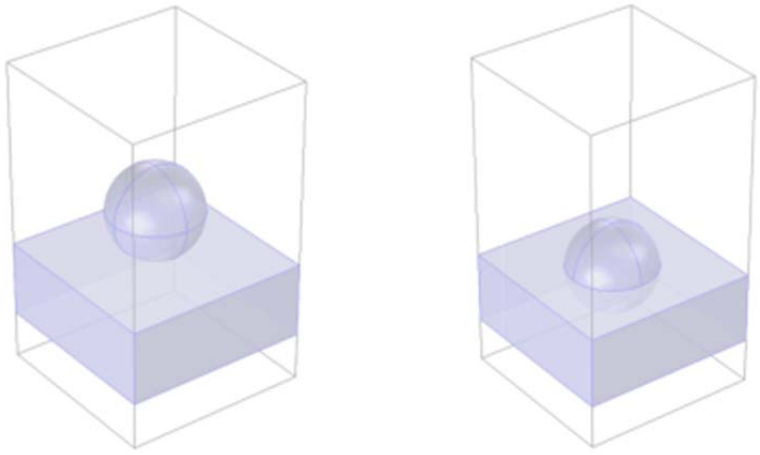

Figure 42 COMSOL Models of One 20 μm Aluminum Sphere in 16 μm of Liquid Tape

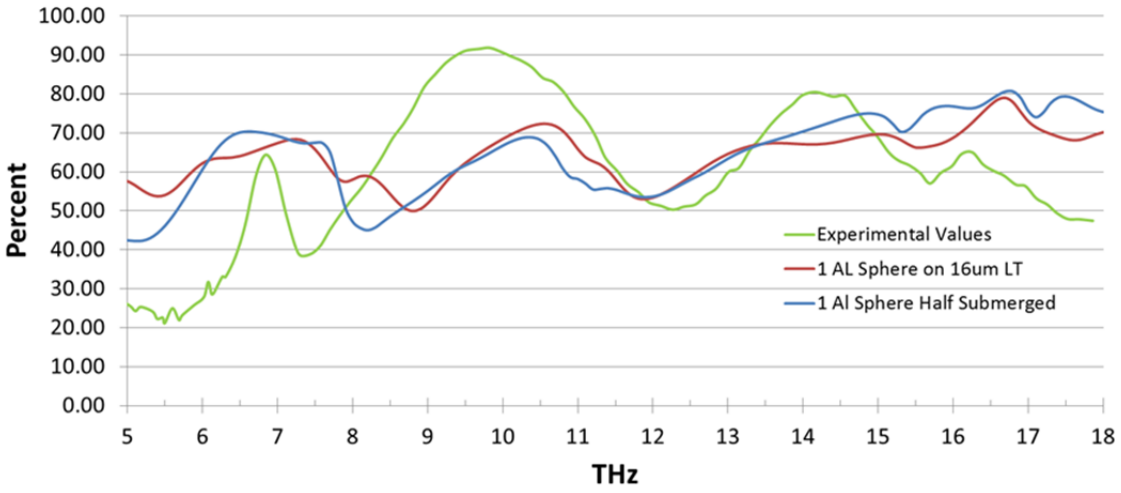

Figure 43 Experimental and COMSOL Results for Absorption in Liquid Tape with 20 μm Diameter Aluminum Spheres

3. Various Numbers of Aluminum Spheres in Photoresist Solution

A series of COMSOL models were built using the SPR955 positive photoresist as a medium for the particles. The models started off with minimal complexity and were incrementally changed to see the effects of varying the parameters. The parameters varied were the number of aluminum particles, the configuration of the aluminum particles, the refractive indices of the photoresist and the aluminum particles, and the conductivity of the aluminum particles.

One property varied through this set of models the treatment of the aluminum spheres. Some of the models were analyzed using the conductivity (σ) of aluminum to solve the finite element model. The value used in this case was $\sigma = 3.8 \times 10^7$ S/m. To use the refractive index values of aluminum, further calculations were required. Experimentally derived values from Ordal et al. were used to derive a 2nd order polynomial equation for n and k that is based on frequency [20]. The equations used were:

$$n_{Al} = 2.13f^2 - 60.24f + 467.28 \quad (15)$$

$$k_{Al} = 1.23f^2 - 42.38f + 490.40 \quad (16)$$

where f is the frequency in THz. The values and graphs used to determine these equations are contained in the Appendix.

Both the real and imaginary portions of the refractive index of the photoresist were calculated using the Thin Film Analysis tools. Due to the frequency dependence of the n and k values, the experimental data was analyzed in 0.5 THz increments and plotted to find equations that represent the frequency dependence. The frequency dependence was minimal for the real portion of refractive index, so a linear fit was used. The imaginary portion had more variance and a third order polynomial was used. The derived equations are Equations (17) and (18):

$$n_{SPR} = 0.0035f + 1.5341 \tag{17}$$

$$k_{SPR} = -0.00003f^3 + 0.00085f^2 - 0.00825f + 0.05096 \tag{18}$$

where f is the frequency in THz. The graphs used to derive these values were discussed previously and can be seen in Figure 37 and Figure 38.

Multiple sets of experimental data were looked at to determine the refractive index of the photoresist and were used for various models in COMSOL. Equations (17) and (18) provided results in COMSOL that were closer to the experimental results. There were differences in the experimental data due to some variance in the thickness of the SPR across the sample and due to the amount of water vapor that had evaporated from the photoresist as the sample was analyzed on multiple days.

The first two models built consisted of two aluminum spheres in a vertical line and then four aluminum spheres aligned in one horizontal plane. These models used a conductivity of 3.8 x 10^7 S/m for aluminum and Equations (17) and (18) for refractive index of the photoresist. The COMSOL values obtained for absorption did not reflect anything close to the experimentally derived values but showed that increasing the number of spheres from two to nine spheres, as seen in Figure 44 brings the model closer to the experimental results.

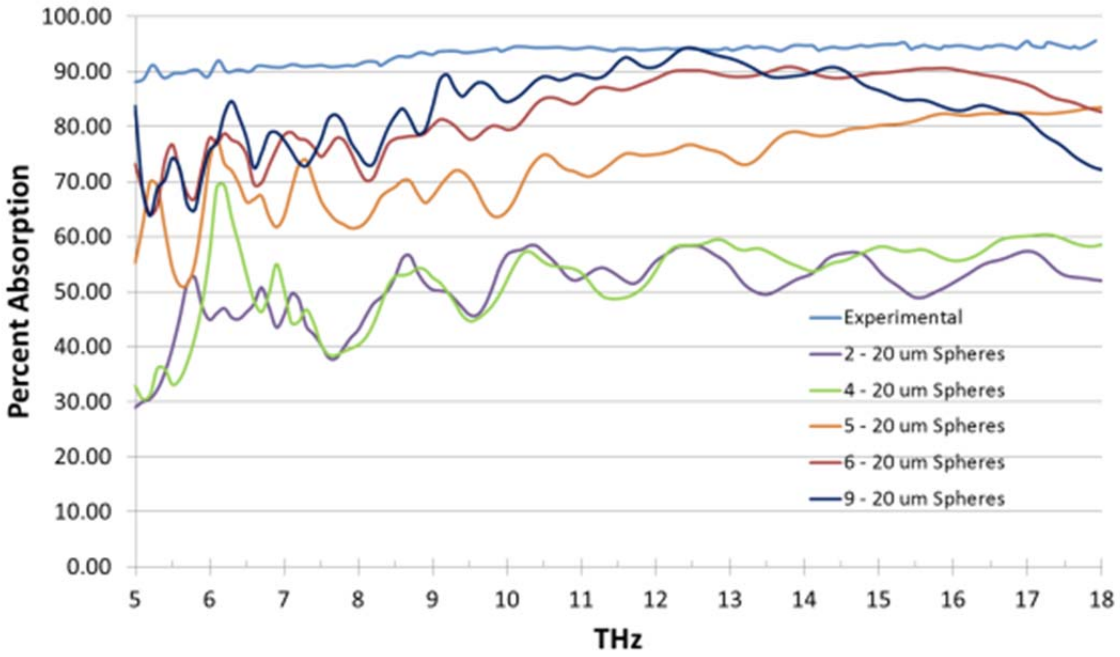

Figure 44 Absorption Characteristics of Two, Four, Five, Six and Nine 20 μm Spheres

Due to the results seen in Figure 48, the results between the six and nine sphere models were fairly similar. In order to strike a balance between computing power and accuracy, the six sphere model was selected to be analyzed in depth and can be seen in Figure 45. The model was built so that there was 20 μm between spheres and 10 μm between the spheres and the boundaries.

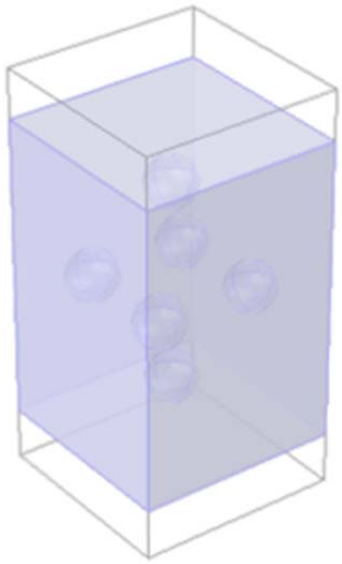

Figure 45 Basic COMSOL Model for Six Aluminum Spheres in Photoresist Solution

The variables analyzed for the six sphere model were a set n and k versus two different frequency dependent refractive index values for the photoresist, and a series of progressively larger aluminum spheres ranging from 20 μm to 40 μm. The spacing between the particles remained constant as the particle size changed. Changing the n and k for the SPR only had the effect of slightly shifting the peaks of the graph. The overall trend of the graph was the same and can be seen in Figure 46.

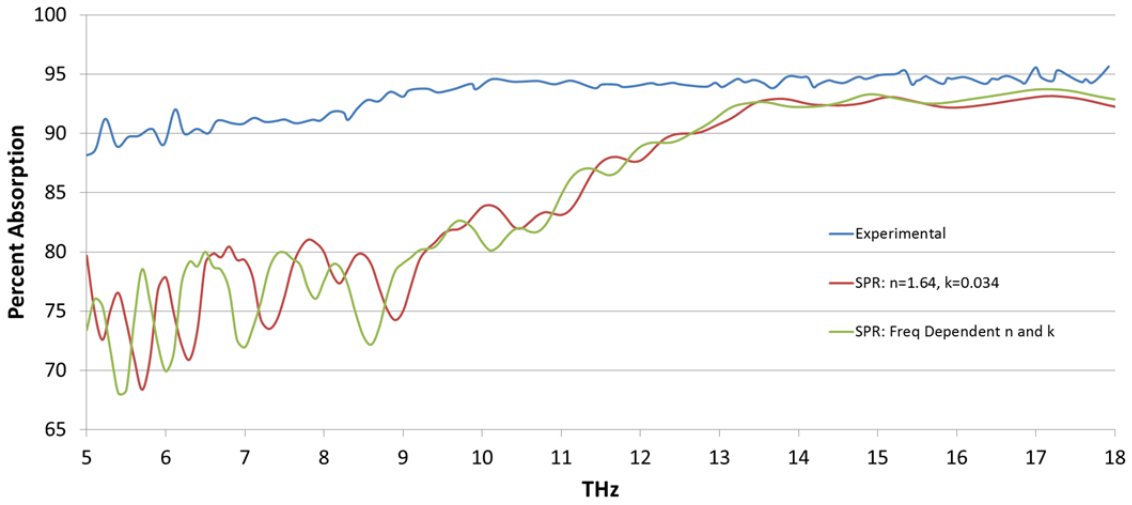

Figure 46 Absorption Characteristics of Six Spheres in Photoresist Utilizing Various Refractive Indices

Changing the sphere sizes had a significant effect on this model. As the spheres got larger, the peak absorption occurred in a lower frequency range seen in Figure 47. The larger spheres absorb more of the lower frequency THZ wave. When a composite graph of the three sphere sizes is constructed, as seen in Figure 48, the model is close to the actual data from 8 to 10.5 THz and a very close match from 10.5 to 18 THz. A cursory analysis of an SEM image, seen in Figure 49, shows that there are particles that are smaller than 5 μm and they are other particles that are larger than 35 μm. Thus, using a variety of sizes of aluminum spheres is a reasonable assumption based on the SEM images taken of the aluminum powder.

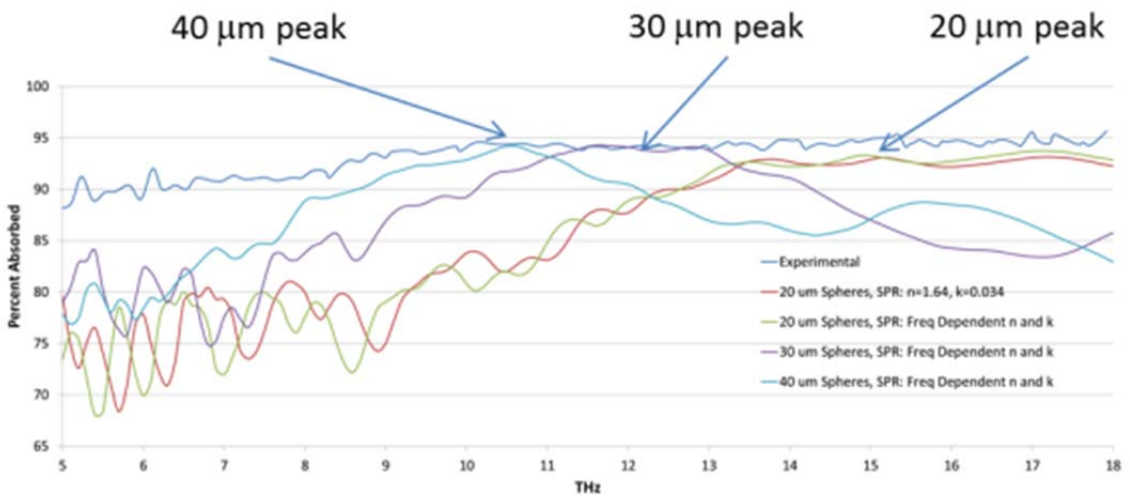

Figure 47 COMSOL Results for the Absorption of Six Aluminum Spheres in Photoresist, with Spheres Ranging from 20 µm to 40 µm

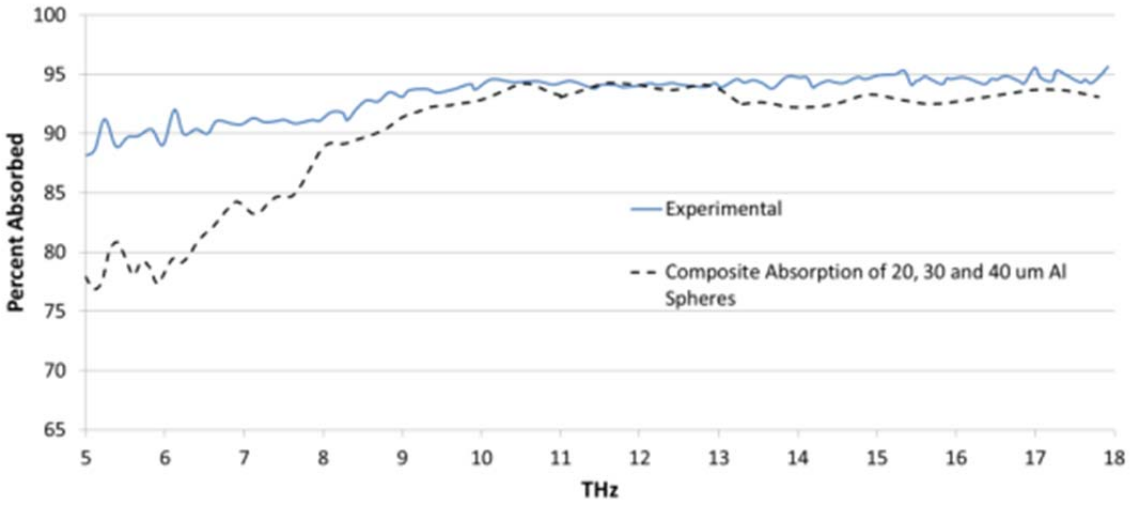

Figure 48 Composite Graph of Absorption Characteristics of 20, 30 and 40 µm Aluminum Spheres

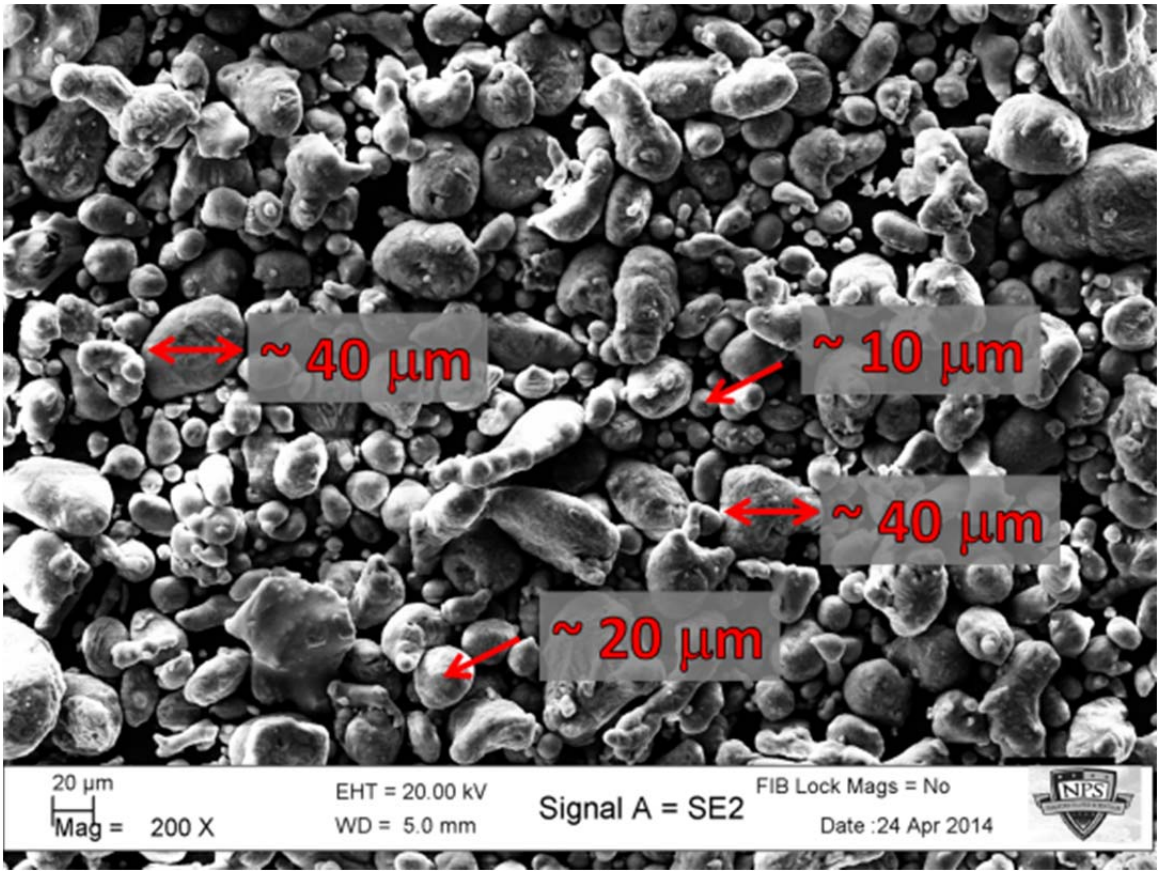

Figure 49 500x SEM Image of Aluminum Powder Showing a Range of Particle Sizes

By changing the sphere size from 20 µm to 40 µm and maintaining the spacing between the spheres, the volume fraction increases from approximately 3.3% aluminum to 5.7% aluminum. Since the overall shape of the graphs is fairly consistent with the exception of shifting the peaks, the change in volume fraction may not have had a large impact on the overall absorption in the models.

Using the COMSOL models, it was also determined that most of the heating occurs in the upper layers of the spheres. Figure 50 depicts the resistive heating losses for the six sphere model at 13 THz and the nine sphere model at 13.8 THz. The frequencies were selected for each case due to the fact that the maximum absorption occurs at the selected frequency for each model. Both models show that most of the THz wave is in the upper layer of spheres due to the heating that occurs there. The bottom layers in both examples show minimal heating. Since the models accurately represented the

experimental results above 10 THz, adding more than three layers of spheres is not likely going to add any more accuracy to the models.

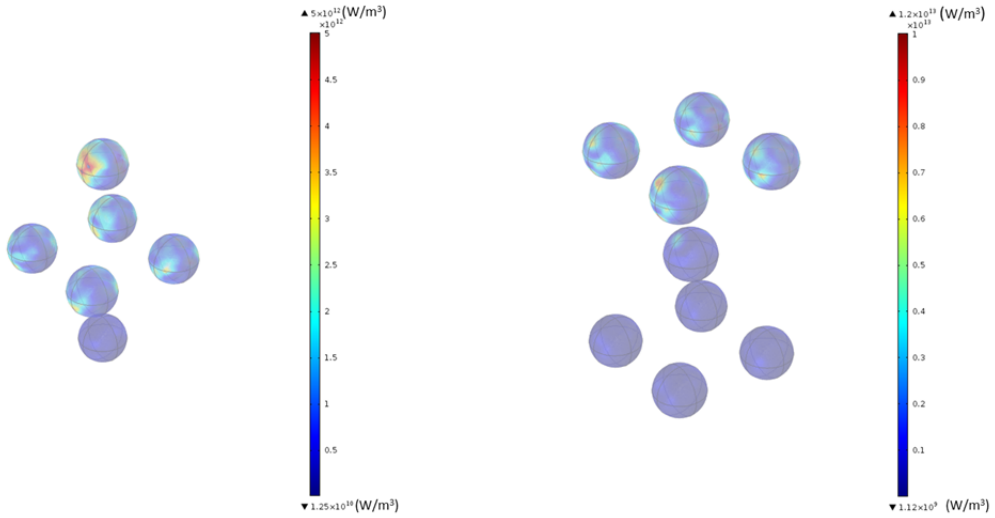

(a) (b)

Figure 50 (a) Resistive Heating Losses (in W/m^3) for Six Spheres at 13 THz
(b) Resistive Heating Losses (in W/m^3)for Nine Spheres at 13.8 THz

THIS PAGE INTENTIONALLY LEFT BLANK

V. CONCLUSIONS

The work in this thesis focused on developing experimental methods to determine the absorption in the THz range of the electromagnetic spectrum of various nano- and micro-sized particles in a variety of media. The results were then used to build and verify finite element models in COMSOL that mirrored the experimentally derived results.

The experimental results showed that epoxy resin exhibits large amounts of absorption between 5 and 18 THz. This made it more difficult to test the absorption characteristics of the CNTs and the nickel particles in epoxy. The liquid tape absorbed much less of the incoming THz wave between 5 and 18 THz, but it proved to be a difficult medium to perform accurate experiment on. The SPR9555 positive photoresist solution did absorb more THz than expected, but the experimental results proved useful in the development of finite element models.

A significant amount of the finite element modeling focused on the aluminum spheres in the SPR955 positive photoresist. The research showed that increasing the number of aluminum particles in a unit cell to six spheres was an accurate representation of the experimental results above 10 THz. The inaccuracy in the model is likely due to a few different factors. One is that there are likely particles and clumps of particles that were larger than 40 μm. Additionally, extremely accurate values for the refractive index of the photoresist were difficult to obtain.

Further research in this area can be conducted to further refine the COMSOL models that currently exist. As previously stated, the weakness is in determining accurate n and k values for the media used. The Fabry-Perot effects seen in the experimentally derived data of all of the samples that used silicon as a substrate made it very difficult to use the tools available for curve fitting due to the periods of oscillations seen on the experimental results. Additionally, the fact that many of the media used displayed a frequency-dependence for both the real and imaginary portions of refractive index added more uncertainty to the values of n and k that were used in the COMSOL models. A

further refinement of the tools used to determine refractive index could greatly enhance the product of the COMSOL models

Additional research, using the refined COMSOL models, can focus on aspects other than the absorption of THz, such as the Joule heating effects. A greater focus on the thermal effects of THz radiation on various composites will allow for better understanding of the physical changes in the composite. The heating of CNTs or micro-particles can have an impact on the strength, hardness and fatigue characteristics of a composite material.

Still further research can be done in trying to build models involving CNTs. The CNTs present a unique challenging in finite element modeling. When CNTs are used in a composite, there are a number of characteristics, such as the length, diameter and chirality that vary for each individual CNT. An efficient way to build and simulate a model capable of accurately representing realistic results is a logical next step for this research.

APPENDIX. DETERMINATION OF REFRACTIVE INDEX FOR ALUMINUM

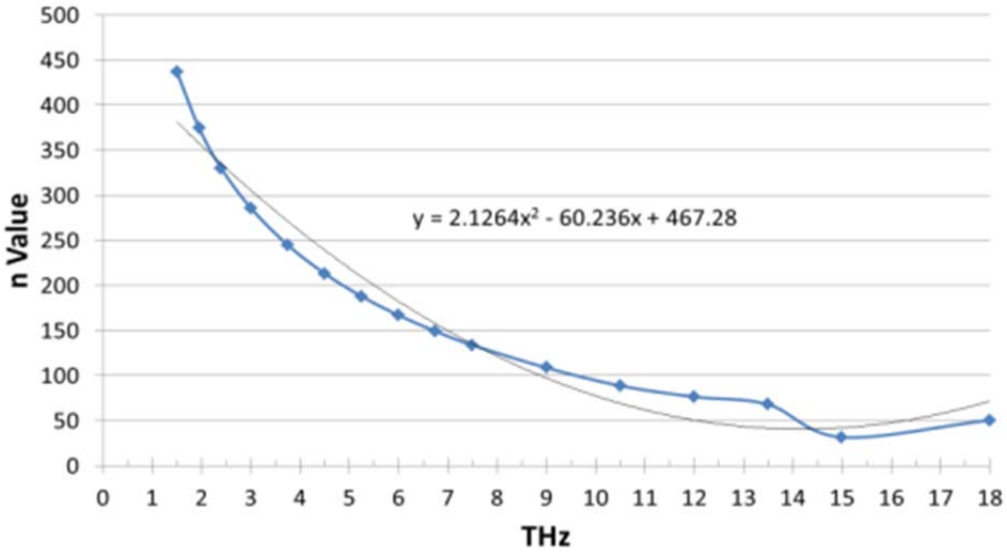

Figure 51 Values and Equations Used for the Real Portion of the Refractive Index of Aluminum

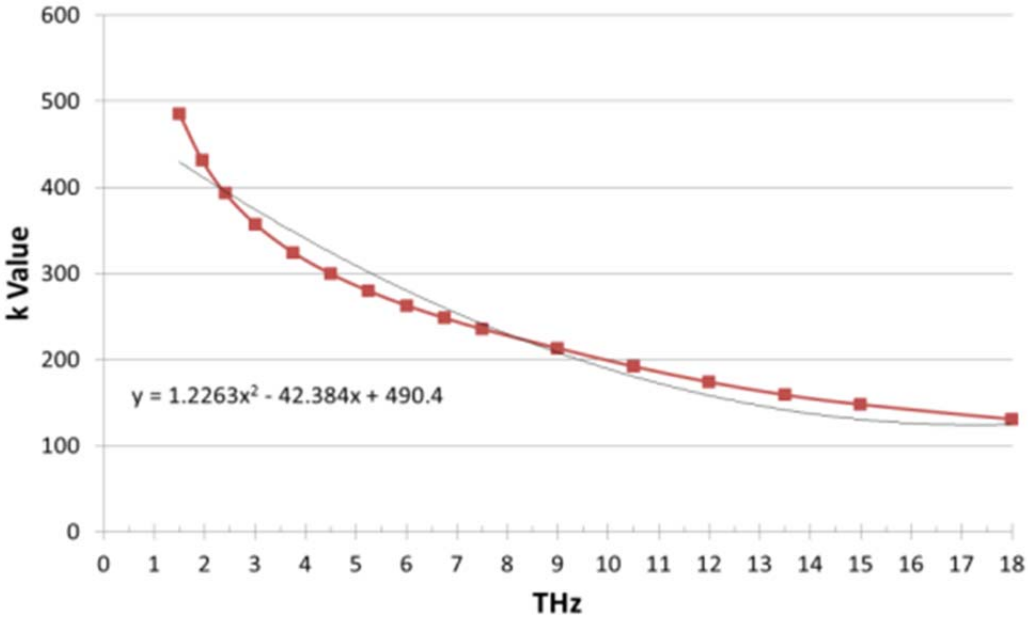

Figure 52 Values and Equations Used for the Imaginary Portion of the Refractive Index of Aluminum

THIS PAGE INTENTIONALLY LEFT BLANK

LIST OF REFERENCES

[1] M. Tonouchi, "Cutting-edge terahertz technology," *Nature Photonics,* vol. I, pp. 97–105, Feb. 2007.

[2] Southern Universities Research Association. (2010, April 7). *6th Annual SURA Terahertz Applications Symp.* [Online]. Available: http://www.sura.org/commercialization/terahertz.html.

[3] S. Iijima, "Helical microtubes of graphitic carbon," *Nature*, vol. 354, pp. 56–58, Nov. 1991.

[4] S. D. Faulkner, "Study of composite joint strength with carbon nanotube reinforcement," M.S. thesis, Dept. Mech. Eng., NPS, Monterey, CA, 2008. Available: http://hdl.handle.net/10945/3995

[5] G. L. Burkholder, "The effects of carbon nanotube reinforcement on adhesive joints for naval applications," M.S. thesis, Dept. Mech. Eng., NPS, Monterey, CA, 2009. Available: http://hdl.handle.net/10945/4378

[6] S. C. Zunjarrao and R. P. Singh, "Characterization of the fracture behavior of epoxy reinforced with nanometer and micrometer sized aluminum particles," *Composites and Sci. Technology,* vol. 66, no. 13, pp. 2296–2305, Oct. 2006.

[7] Y. Sun *et al.*, "Design and development of new nano-reinforced bonds and interfaces," in *Nanotech 2004 The Nanotechnology Conference and Trade Show*, Boston, MA., 2004, vol. 3, pp. 126–129.

[8] J. Bell *et al.*, "Polymer-carbon nanotube composites: Basic science and applications," *Materials Forum,* vol. 32, pp. 144–152, 2008.

[9] J. Robertson, "Realistic applications of CNTs," *Materials Today*, vol. 7, no. 10, pp. 46–52, Oct. 2004.

[10] J. W. Downs, "Novel synthesis of 3D Graphene-CNF electrode architectures for supercapacitor applications," M.S. thesis, Dept. Mech. Eng., NPS, Monterey, CA, 2012. Available: http://hdl.handle.net/10945/34659

[11] M. Martin *et al.*, "Mechanical behavior of nickel + aluminum powder-reinforced epoxy composites," *Materials Sci. and Eng.,* vol. 443, no. 1–2, pp. 207–218, Aug. 2007.

[12] I. Hosako *et al.*, "At the dawn of a new era in terahertz technology," *Proc. IEEE,* vol. 95, pp. 1611–1623, Aug. 2007.

[13] D. Grbovic *et al.*, "Optimization of THz absorption in thin films," *Proc. 2011 IEEE Sensors*, Limerick, 2011, pp. 172–175.

[14] F. Alves *et al*., "Highly absorbing nano-scale metal films for terahertz applications," *Optical Engineering,* vol. 51, no. 6, June 2012.

[15] *Nexus FTIR Spectrometers: 870 User's Guide,* Madison, Wi: Nicolet Instrument Company, 1999.

[16] *MappIR Automated Sampling Accessory: Installation and User* Guide, Pike Technologies, 2013.

[17] F. L. Pedrotti and L. S. Pedrotti, *Introduction to Optics*, Upper Saddle River, NJ: Prentice-Hall, 1993.

[18] M. F. Martin, "An efficient method to obtain the optical properties of multilayered media in the terahertz range," M.S. thesis, Dept. Mech. Eng., NPS, Monterey, CA, 2013.

[19] F. Alves *et al*., "Strong terahertz absorption using SiO2/Al based metamaterial structures," *Applied Physics Letters,* vol. 100, no. 11, p. 111104, 2012.

[20] M. A. Ordal *et al.*, "Optical properties of Al, Fe, Ti, Ta, W, and Mo at submillimeter wavelengths," *Applied Optics,* vol. 27, no. 6, pp. 1203–1209, 1988.

INITIAL DISTRIBUTION LIST

1. Defense Technical Information Center
   Ft. Belvoir, Virginia

2. Dudley Knox Library
   Naval Postgraduate School
   Monterey, California